Characterisation of Reference Materials for In situ Rb-Sr Dating by LA-ICP-MS/MS

Yujin Jegal, Catherine Zimmermann, Laurie Reisberg, Delphine Yeghicheyan, Christophe Cloquet, Chantal Peiffert, Marie Gerardin, Etienne Deloule, J. Mercadier

Characterisation of Reference Materials for *In situ* Rb-Sr Dating by LA-ICP-MS/MS

Yujin **Jegal** (1, 2)*, Catherine **Zimmermann** (1), Laurie **Reisberg** (1), Delphine **Yeghicheyan** (1), Christophe **Cloquet** (1), Chantal **Peiffert** (2), Marie **Gerardin** (2), Etienne **Deloule** (1) and Julien **Mercadier** (2)

(1) Université de Lorraine, CNRS, CRPG, UMR 7358, 54500 Vandoeuvre-lès-Nancy, France

(2) Université de Lorraine, CNRS, GeoRessources, 54506 Vandoeuvre-lès-Nancy, France

*Corresponding author. e-mail: yujin.jegal@univ-lorraine.fr

Abstract

We present here Rb and Sr mass fractions and $^{87}Sr/^{86}Sr$ compositions for four reference materials (RM) obtained from the Service d'Analyse des Roches et des Minéraux (SARM) in Nancy, France: Mica-Mg, Mica-Fe, GL-O and FK-N. These four RMs have different chemical compositions spanning the range of those of most K-bearing feldspars and micas, making them potential calibration materials for *in situ* Rb-Sr dating of natural minerals by LA-ICP-MS/MS. Selected grains and flakes from the four RMs present variable degrees of heterogeneity observable by SEM-EDS and EPMA imaging and chemical mapping. This heterogeneity is mainly related to inclusions of minerals within flakes and grains and to chemical substitutions linked to crystallographic control and alteration processes. The Mica-Mg RM is the least affected. The powders available at the SARM were analysed by ID-TIMS ($^{87}Sr/^{86}Sr$ and Sr mass fractions) and ID-MC-ICP-MS (Rb) after digestion and separation. The mean $^{87}Rb/^{86}Sr$ ratios are 155.6 ± 4.7% (2*s*, as for other RMs) for Mica-Mg, 1815 ± 14% for Mica-Fe, 36.2 ± 11% for GL-O and 69.9 ± 5.9% for FK-N. The mean $^{87}Sr/^{86}Sr$ ratios are 1.8622 ± 0.36% (2*s*, as for other RMs) for Mica-Mg, 7.99 ± 13% for Mica-Fe, 0.75305 ± 0.12% for GL-O, and 1.2114 ± 0.17% for FK-N. The four RMs each show dispersion in $^{87}Sr/^{86}Sr$ and Rb and Sr mass fractions, to degrees that differ between RMs and that reflect the heterogeneity of their original crystals. The most

heterogeneous RMs are GL-O and Mica-Fe. The calculated mean Rb-Sr isotopic ages are 521 ± 24 Ma for Mica-Mg, 287 ± 55 Ma for Mica-Fe, 89.2 ± 9.9 Ma for GL-O and 512 ± 30 Ma for FK-N. The proposed age for Mica-Fe may be unreliable due to the elevated dispersion of individual analysis linked to the highly radiogenic composition of the biotite and to the presence of numerous mineral inclusions. We recommend use of these proposed working values of $^{87}Sr/^{86}Sr$ and $^{87}Rb/^{86}Sr$ ratios and associated uncertainties when using the four RMs for *in situ* Rb-Sr dating by LA-ICP-MS/MS. The availability of these four well-characterised RM will allow progress in the development and application of the Rb-Sr dating approach by LA-ICP-MS/MS.

Keywords: Rb-Sr dating, LA-ICP-MS/MS, reference material, *in situ*, mica, feldspar.

Received 27 Feb 22 – Accepted 23 Jul 22

The Rb-Sr geochronometer (see summary in Nebel 2014) has been widely used for decades to date and constrain the cooling history of geological events based on the Rb-Sr decay system. In this system ^{87}Rb undergoes β- decay to ^{87}Sr with a constant of $1.3972 \pm 0.0045 \times 10^{-11}$ a^{-1} (Villa *et al.* 2015), corresponding to a half-life of ~ 49.6 Ga. Rubidium is a common element in numerous minerals, such as K-rich phases in which Rb^{1+} substitutes for K^{1+}. The Rb-Sr dating method is particularly useful for rocks that lack minerals such as zircons or monazite that are datable using the U-Pb radiometric couple. To define Rb-Sr isochrons, $^{87}Rb/^{86}Sr$ and $^{87}Sr/^{86}Sr$ ratios have been traditionally measured in co-genetic minerals and/or whole rock powders (Armstrong *et al.* 1966, Freeman *et al.* 1997, Glodny *et al.* 2002, Glodny *et al.* 2008, Walawender *et al.* 1990) by conventional isotope dilution thermal ionisation mass spectrometry (TIMS) or multi collector inductively coupled plasma-mass spectrometry (MC-ICP-MS) with a precision (2*s*) of ca. 0.1–0.2% for Rb/Sr measurements (Nebel and Mezger 2006, Nebel *et al.* 2005, Waight *et al.* 2002, Willigers *et al.* 2004). Quadrupole based ICP-MS (ICP-QMS) has also been used for $^{87}Sr/^{86}Sr$ isotope ratio measurement when high-precision is not required (Vanhaecke *et al.* 1999). To measure $^{87}Rb/^{86}Sr$ and $^{87}Sr/^{86}Sr$ ratios in co-genetic pure mineral

separates by these analytical approaches, samples need to be initially prepared by crushing followed by extraction of minerals by hand-picking or mineral separation (Chen *et al.* 1996, Eberlei *et al.* 2015, Farina *et al.* 2014, Fletcher *et al.* 1997, Li *et al.* 2005). The dissolution of mineral separates and/or powders is followed by the chemical separation of Rb from Sr using extraction chromatography, which is required to remove isobaric interference of ^{87}Rb on ^{87}Sr. Conventional Rb-Sr dating using digestion and wet chemistry methods is consequently analytically time-consuming, and could moreover be affected by geological and mineralogical limitations that perturb the isotopic systems of target minerals, such as inclusions, alteration and/or complex age zonation.

Recently, the use of tandem ICP mass spectrometers (ICP-MS/MS) associated with suitable reaction gases (O_2, N_2O, SF_6 or CH_3F) has been demonstrated to be a promising approach for resolving the ^{87}Rb-^{87}Sr isobaric overlap without prior Rb-Sr chemical separation (Bolea-Fernandez *et al.* 2016a, Liu *et al.* 2020). These results are based on initial work by Moens *et al*. (2001) that demonstrated that Sr^+ selectively reacts with CH_3F in an ICP-MS equipped with a dynamic reaction cell (DRS) by forming SrF^+ ions. The experimental study of Cheng *et al*. (2008) reported that Sr^+ is much more reactive than Rb^+ with CH_3F or SF_6, forming SrF^+ by F-atom transfer, and with N_2O or O_2, forming SrO^+ by O-atom transfer. The coupling of a laser ablation (LA) system with such ICP-MS/MS associated with appropriately selected reaction gases now allows *in situ* Rb-Sr dating of geological samples with short sample preparation and analytical times, and precisions of ca. 1.0–2.5% for Rb-Sr dating (Gorojovsky and Alard 2020, Hogmalm *et al.* 2017, Redaa *et al.* 2021, Zack and Hogmalm 2016). This new approach avoids the drawbacks of the bulk Rb-Sr method and is revolutionising the application of Rb-Sr age dating in geosciences. Its use has increased over the past few years for geochronological analyses of K-bearing mica and/or feldspar minerals in various case studies: in hydrothermal vein and fault systems (Tillberg *et al.* 2017, Tillberg *et al.* 2020), in ore (Olierook *et al.* 2020, Şengün *et al.* 2019) and mineral deposits (Redaa *et al.* 2021), for kimberlites (Gorojovsky and Alard 2020), and for the characterisation of Archaean to Proterozoic crustal rocks (Li *et al.* 2020).

The *in situ* Rb-Sr dating method by LA-ICP-MS/MS, however, currently faces some challenges that limit the accuracy and precision of the measured ^{87}Sr-^{86}Sr and ^{87}Rb-^{86}Sr ratios and related Rb-Sr ages. Among these limitations, the main ones are elemental and isotopic fractionation and matrix effects. Such effects during LA-ICP-MS analysis of other elemental and isotope systems have been investigated by many studies (e.g., Claverie *et al.* 2009, Jackson and Günther 2003, Jackson and Sylvester 2008, Liu *et al.* 2013, Rodushkin *et al.* 2002, Zhang *et al.* 2016 among others) and recently have been documented for LA-ICP-MS/MS analysis applied to Rb-Sr dating (Gorojovsky and Alard 2020, Redaa *et al.* 2021). Gorojovsky and Alard (2020) showed that the use of reference materials (RMs) with diverse matrices using different laser systems and conditions can significantly affect the accuracy of $^{87}Sr/^{86}Sr$ and $^{87}Rb/^{86}Sr$ ratios of selected minerals and thus their calculated Rb-Sr ages. Redaa *et al.* (2021) also reported that different ablation parameters and contrasts between the physical properties of nano-powder pellet and glass RMs and phlogopites can influence the accuracy of the obtained Rb-Sr ages. Measurements of $^{87}Sr/^{86}Sr$ and $^{87}Rb/^{86}Sr$ ratios by LA-ICP-MS/MS consequently require use of the same analytical conditions and external calibration using RMs with physical and chemical properties similar to those of the unknown natural samples (Hogmalm *et al*. 2017, Zack and Hogmalm 2016). Thus, homogeneous RMs with well-characterised Rb/Sr ratios and Sr isotope compositions are crucial for accurate calibration of LA-ICP-MS/MS systems when used for *in situ* Rb-Sr geochronology. Unfortunately, the availability of suitable RMs is limited. As a result, synthetic reference glasses such as NIST SRM 610 or 612 have been widely used as primary calibration standards for *in situ* measurements of $^{87}Sr/^{86}Sr$ values of geological reference glasses and natural minerals (Bolea-Fernandez *et al.* 2016b, Gorojovsky and Alard 2020, Hogmalm *et al.* 2017, Li *et al.* 2020, Olierook *et al.* 2020, Redaa *et al.* 2021, Şengün *et al.* 2019, Zack and Hogmalm 2016). NIST SRM 612 and USGS BCR-2G or USGS BHVO-2G, although subject to matrix effects, have also been used to calibrate $^{87}Rb/^{86}Sr$ ratios of natural minerals such as feldspars (Gorojovsky and Alard 2020, Tillberg *et al.* 2020, Zack and Hogmalm 2016). The CRPG phlogopite Mica-Mg (Govindaraju 1979) is currently used as a RM to calibrate $^{87}Rb/^{86}Sr$ ratios of micas (Gorojovsky and Alard 2020, Hogmalm *et al.* 2017, Li *et al.* 2020, Olierook *et al.* 2020, Redaa *et al.* 2021, Rösel and Zack 2021,

Şengün *et al.* 2019), using the $^{87}Rb/^{86}Sr$ values for Mica-Mg proposed by Hogmalm *et al.* (2017). While this alleviates concerns about matrix effects, it raises the issue of possible Rb/Sr heterogeneity in this natural material. In the study of Hogmalm *et al.* (2017), the $^{87}Sr/^{86}Sr$ ratio of Mica-Mg was measured and calibrated relative to NIST SRM 610 by LA-ICP-MS/MS, and the $^{87}Rb/^{86}Sr$ ratio was calculated using the mean of the reported ages (519.4 ± 6.5 Ma) in the Bekily area of Madagascar where the Mica-Mg phlogopite was collected, coupled with an initial ratio of 0.72607 ± 0.00070 from Morteani *et al.* (2013). The homogeneity of Mica-Mg is currently unknown, and true $^{87}Sr/^{86}Sr$ and $^{87}Rb/^{86}Sr$ values are not yet characterised. More broadly, the development and distribution of matrix-matched RMs are critical to expanding the application of *in situ* Rb-Sr dating to minerals, such as micas and feldspars, covering various matrices and a wide range of $^{87}Sr/^{86}Sr$ and $^{87}Rb/^{86}Sr$.

Therefore, the aim of this work is to characterise and establish RMs suitable for *in situ* Rb-Sr geochronology of micas and feldspars by LA-ICP-MS/MS. Four RMs, phlogopite Mica-Mg, biotite Mica-Fe, glauconite GL-O and potassium feldspar FK-N, were obtained from the Service d'Analyse des Roches et des Minéraux (SARM) of the CRPG laboratory in Nancy, France. The nature and homogeneity of the RMs were first investigated by imaging and elemental mapping of the mineral grains before powdering. Isotope dilution MC-ICP-MS and TIMS were performed to determine $^{87}Sr/^{86}Sr$ and $^{87}Rb/^{86}Sr$ ratios for these four RMs using different powder batches. Based on the results, recommended values of these parameters and related absolute ages are proposed.

Sample selection

The RMs in this study were selected based on their compositional variation which spans a large range in Rb/Sr ratios (12–440), covering the global chemical composition of micas and feldspars from different locations compiled in the Georoc database (Figure 1). They include a phlogopite (Mica-Mg), a biotite (Mica-Fe), a glauconite (GL-O) and a potassium feldspar (FK-N), which are certified for their chemical composition and distributed by the SARM (Service d'Analyse des Roches et des

Minéraux, CNRS National facility; https://sarm.cnrs.fr/), located at the Centre de Recherches Pétrographiques et Géochimiques (CRPG, Nancy, France). Details of the sample collection, preparation, and working values of the RMs were reported by Govindaraju (1979, 1984, 1995) and Odin *et al*. (1982) and the RMs are available on request. Phlogopite Mica-Mg originates from a phlogopite deposit of the Bekily area, southern Madagascar (Govindaraju 1979). Biotite Mica-Fe is extracted from biotite emplaced in magmatic shear zones within the Saint-Sylvestre two mica leucogranitic complex near Razès, France (Govindaraju 1979; Friedrich 1983). Glauconite GL-O was sampled from a calcareous and glauconitic sand in the basal Cenomanian section in the Cauville cliff, Normandy, France (Odin *et al*. 1982). Potassium feldspar FK-N is from Tamil Nadu, India (Govindaraju 1984). Brief descriptions of reported geochronological data for the four RMs are presented in Table 1. The reported ages range from 503 ± 15 to 528 ± 9 Ma for Mica-Mg, from 307.6 ± 0.4 to 321 ± 10 Ma for Mica-Fe, and from 80.9 to 98.2 Ma for GL-O. Precise sample location and age data for the FK-N RM have not been reported (Govindaraju 1984), but a Rb-Sr age based on samples from leucogranites and pegmatites from Tamil Nadu considered to be co-genetic with FK-N was proposed (521 ± 9 Ma; Pandey *et al*. 1993).

In this work, all four RMs were investigated in powder form and as mineral grains for GL-O and FK-N and flakes for Mica-Mg and Mica-Fe (**Table S1**). The powdered RMs were provided by the SARM in the form of three bags (10 g each) for Mica-Mg and Mica-Fe and as aliquots of less than 5 g for GL-O and FK-N. A 10 g bag is the conventional form of distribution of RM by the SARM. Multiple powder batches (50-110 mg for each batch) from the different bags and aliquots were analysed by isotope dilution TIMS and MC-ICP-MS. Multiple powder batches (200 mg) of the RMs were also analysed by alkali fusion ICP-MS. The powder batches for alkali fusion ICP-MS analyses were from three bags (10–20 g) for each of the RM, which are different from the bags and aliquots used for ID-TIMS and MC-ICP-MS analyses. Additionally, several grains (GL-O and FK-N) and flakes (Mica-Mg and Mica-Fe) were randomly selected and investigated by SEM-EDS and EPMA. For simplicity,

the form of the four RMs analysed by SEM-EDS and EPMA is indicated as “grains” in the rest of this work.

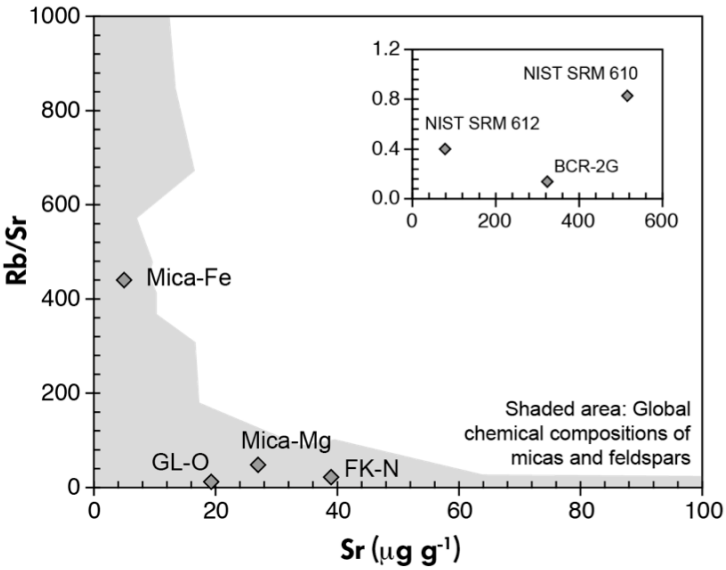

Figure 1. Rb/Sr and Sr (µg g^{-1}) diagram showing the accepted working values (Govindaraju 1995) for the four Reference Materials (Mica-Mg, Mica-Fe, GL-O and FK-N) used in this study. Inset shows these values for the Certified Reference Materials NIST SRM 610, NIST SRM 612 and BCR-2G (Wise and Watters 2012, Woodhead and Hergt 2001, Elburg *et al.* 2005) used in previous LA-ICP-MS/MS studies of Rb-Sr dating of natural minerals. Note the difference in Sr and Rb/Sr scales relative to the main figure. Grey shaded area indicates the chemical compositions of micas and feldspars from different locations compiled in the georoc database (http://www.georoc.mpch-mainz.gwdg.de/).

Table 1.
Previously reported ages for the samples and for their host rocks or associated deposits with Rb-Sr model ages of the samples in this study

Sample	Age (Ma)	Reference	Method
Mica-Mg	524.7 ± 2.7	Zimmermann *et al.* (1985)	K-Ar of Mica-Mg flakes
	503 ± 15[a]	Govindaraju (1979)	Rb-Sr of Mica-Mg
	522 ± 12	Govindaraju (1979)	K-Ar of Mica-Mg flakes
	528 ± 9.37	Laureijs *et al.* (2021)	Rb-Sr of Mica-Mg powder

	526 ± 34	Kröner *et al.* (1996)	U-Pb of zircon lower interception from K-feldspar gneiss from Ihosy quarry, southern Madagascar
	518 ± 8[a]	Morteani *et al.* (2013)	Rb-Sr of phlogopites from the pegmatites, Ampandrandrava, southern Madagascar
	499 ± 10[a]	Martin *et al.* (2014)	Rb-Sr of calcite-phlogopite from the Sakamasy deposit, southern Madagascar
	500 ± 10[a]	Martin *et al.* (2014)	Rb-Sr of calcite-phlogopite from the Sakaravy deposit, southern Madagascar
	521 ± 24[b]	this study	Rb-Sr of Mica-Mg by ID-TIMS and MC-ICP-MS[b]
GL-O	80.9–98.2[a]	Odin *et al*. (1982)	Rb-Sr of GL-O powder
	87.5–95.6[a]	Odin *et al.* (1982)	Rb-Sr of GL-O grains
	93.1–96.7[a]	Odin *et al.* (1982)	K-Ar of GL-O grains
	95.8–88.3[a]	Smith *et al.* (1998)	Ar-Ar of GL-O grains
	89.2 ± 9.9[b]	this study	Rb-Sr of GL-O by ID-TIMS and MC-ICP-MS[b]
Mica-Fe	315.9 ± 8.5	Zimmermann *et al*. (1985)	K-Ar of Mica-Fe flakes
	321 ± 10[a]	Govindaraju (1979)	Rb-Sr of Mica-Fe
	310 ± 10	Govindaraju (1979)	K-Ar of Mica-Fe
	307.6 ± 0.4	Grouve and Harrison (1996)	Ar-Ar of Mica-Fe flakes
	324 ± 4	Holliger *et al.* (1986)	U-Pb upper intercept age of monazite and zircon from the western part of the Massif of Saint-Sylvestre
	320.1 ± 18.3[a]	Duthou (1977)	Rb-Sr of whole-rock, leucogranite of Saint-Sylvestre
	302.10 ± 0.87	Scaillet *et al.* (1996)	Ar-Ar plateau age obtained on muscovites from the granite of Saint-Sylvestre
	302.44 ± 063	Scaillet *et al.* (1996)	Ar-Ar plateau age (biotites) from Saint-Sylvestre granite
	301.44 ± 0.65	Scaillet *et al.* (1996)	
	287 ± 55[b]	this study	Rb-Sr of Mica-Fe by ID-TIMS and MC-ICP-MS[b]
FK-N	521 ± 9[a]	Pandey *et al.* (1993)	Rb-Sr of leucogranite and alkali feldspar pegmatite granite in Tamil Nadu, India
	512 ± 30[b]	this study	Rb-Sr of FK-N by ID-TIMS and MC-ICP-MS[b]

[a] Recalculated using revised ^{87}Rb decay constant of Villa *et al*. (2015)

[b] Rb-Sr model ages calculated from the mean Rb-Sr isotopic values and total uncertainties by ID-TIMS and MC-ICP-MS and assumed initial Sr ratio. Details of the calculation are described in section 5.3.

Analytical methods

3.1. SEM-EDS and EPMA

Several grains from the four RMs were randomly selected and embedded in epoxy resin, abraded and polished. Polished sections were carbon coated for scanning electron microscope (SEM) and electron microprobe analysis (EPMA). A TESCAN VEGA3 SEM equipped with an EDS (Bruker Xflash6 30 mm^2) was used for mineralogical observations at the Service Commun de Microscopie Electronique et de Microanalyses (SCMEM) of the GeoRessources laboratory (Vandoeuvre-lès-Nancy, France). Backscattered electron (BSE) images were obtained with an accelerating voltage of 15 kV, a beam current of 10 nA and a working distance of 15 mm. Major element compositions were determined by EPMA (CAMECA SX100) equipped with wavelength dispersive spectrometers (WDS) at the SCMEM of the GeoRessources laboratory. An accelerating of voltage of 15 kV and a beam current of 12 nA were used with a counting time of 10 s per element. X-ray element distribution maps by SEM-EDS were acquired with a dwell time of 16.384 ms per pixel and an image resolution of 512 x 512 pixels. X-ray maps by EPMA were obtained using a step size of 5–9 µm, dwell time of 200 ms, accelerating voltage of 15 kV, current at 100 nA and a beam diameter of 1 µm.

3.2. Alkali fusion ICP-MS

The four RMs powders were analysed by ICP-MS measurements using the alkali fusion technique applied routinely at the SARM adapted from the procedure of Carignan *et al.* (2001). Briefly, 200 mg were weighted in a Pt crucible and mixed with 600 mg of ultrapure $LiBO_2$. Ultra-pure $LiBO_2$ is produced from pure lithium carbonate and boric acid at the SARM, allowing much lower blank levels to be attained than with commercially available $LiBO_2$. The samples were progressively heated to 980 °C and maintained for about 40 min at this temperature. The resulting fused beads were cooled at room temperature before dissolution of the glass in a solution containing 0.5 mol l^{-1} HNO_3 and distilled glycerol, which serves as a wetting agent. Dilution of the resultant solution by a factor of 10 was done in Teflon vials before analysis using an iCAP Q ICP-MS (Thermo Fisher Scientific). Lithium, Rh and Re were used as internal standard elements for the measurements. Each RM was

sampled from three different 10 g bags and two powder aliquots were digested from each bag (Table S1). Each digestion was measured three times to give a total of eighteen measurements for each material. The Sr and Rb contents (µg g^{-1}) in batches of $LiBO_2$ ranged from 0.005 to 0.065 and from 0.010 to 0.050, respectively, which would thus contribute < ~ 3.3% (Mica-Fe) and < ~ 1% (other RM) of the total Sr and < ~ 0.3% (BE-N) and < ~ 0.1% (other RM) of the total Rb present in the samples.

3.3. Isotope dilution TIMS and MC-ICP-MS

3.3.1. Spike calibration: The ^{84}Sr-enriched (99.64%) and ^{85}Rb-enriched (99.77%) isotope tracers (spikes) from Oak Ridge Laboratory (ORNL, Tennessee, USA) were prepared separately. The isotopic composition of the Sr spike reported in assays provided by ORNL in 1999 was used in this work. The Rb isotopic compositions of the Rb spikes were measured in this study using a Neptune Plus MC-ICP-MS at CRPG. For calibration of the Rb spike concentration, the ASTASOL® standard solution (Analytica®, spol. s.r.o.) of 1000 ± 2 mg l^{-1} Rb was diluted to 10 µg ml^{-1} solution in 2% HNO_3 then mixed with the spike solution in spike/standard weight ratios ranging from ca. 0.22 to 0.30. The Sr spikes were calibrated using the standard from NIST SRM 987 powder dissolved and diluted to 10 µg/g solution in 2% HNO_3 using spike/standard weight ratios of 1.6 to 8.2. Isotope analyses of the mixtures were performed using a Neptune Plus MC-ICP-MS for Rb and a TRITON Plus thermal ionisation instrument (TIMS) for Sr at CRPG. Replicate calibrations yield values for ^{84}Sr (M/g) of 3.53 x 10^{-8} ± 0.66% for Spk-3 and 7.03 x 10^{-9} ± 0.47% for Spk-4 and values for ^{85}Rb (M/g) of 9.36 x 10^{-6} ± 1.9% for Spk-1 and 1.98 x 10^{-7} ± 1.7% for Spk-2 (all total uncertainties 2*s*%, Table 2). The total uncertainties (2*s*%) of the Rb spikes presented in Table 2 are dominated by the uncertainties associated with the replicate calibrations but also include the uncertainties on the ASTASOL solution.

Table 2.
^{85}Rb and ^{84}Sr (M/g) of the ^{85}Rb and ^{84}Sr spikes, respectively, and uncertainties (2 SD%) from replicate spike calibration measurements. The uncertainties of the Rb spikes are total values that include both the variation of replicate spike calibration measurements and uncertainties on the concentrations of the solutions used for calibration. The ^{85}Rb and ^{84}Sr spikes were added separately in differing amounts depending on the sample composition.

Spike	M/g	2 SD (%)	Spiked samples
Rb Spike			
Spk-1	9.36×10^{-6}	1.9	Mica-Mg, Mica-Fe, GL-O, FK-N, SRM-607, GA
Spk-2	1.98×10^{-7}	1.7	BE-N
Sr Spike			
Spk-3	3.53×10^{-8}	0.66	Mica-Mg, GA, BE-N
Spk-4	7.03×10^{-9}	0.47	Mica-Fe, GL-O, FK-N, SRM-607

Spike calibration uncertainties of the Rb spikes include both 2 SD (two standard deviation) variation of replicate analyses and uncertainties on the concentration of the standard used for calibration.

3.3.2. Chemistry and analyses: Digestion, chemical separation, and purification were performed in laminar flow hoods in a clean laboratory with filtered air at CRPG. To determine the Rb-Sr isotopic composition of the powdered RMs, multiple batches from aliquots of SARM sample bags (Table S1) were analysed using 50 to 110 mg for each analysis. The sample powders were doped with calibrated ^{85}Rb-enriched and ^{84}Sr-enriched spikes, with the amount of each spike dependent on the sample composition (Table 2). The samples were then dissolved in a mixture of 1.5 ml ultra-pure HF (Seastar Chemicals) and 1.5 ml concentrated HNO_3 (67–69%, PlasmaPURE Plus Acids) on a hot plate (120 °C) for about 48 h. Samples were dried at 110 °C and refluxed with 3 ml of ultra-pure 6 mol l^{-1} HCl (Seastar Chemicals) at 120 °C for more than 48 h to dissolve fluorides precipitated during the first dissolution. After drying, 1 ml of 2.5 mol l^{-1} HCl was added to each beaker, and the samples were centrifuged in 1-ml plastic centrifuge tubes. Next, 0.5 ml of the resulting solution was loaded on cation exchange resin (AG-50X8) columns for Rb and Sr separation and removal of the matrix. The Sr fractions were purified by loading again on the same columns after cleaning the resin with 6 mol l^{-1} HCl and purified water. This procedure resulted in Rb and Sr fractions with only small isobaric interferences (^{85}Rb/^{86}Sr < 0.0001 for Sr determinations by TIMS; ^{88}Sr/^{85}Rb < 0.0002 (^{86}Sr/^{85}Rb < 0.00001) for Rb determinations by MC-ICP-MS).

Strontium isotopic compositions were measured using a TRITON Plus TIMS at CRPG. Mass fractionation was corrected using an exponential law and assuming a natural ^{86}Sr/^{88}Sr ratio of 0.1194

for normalisation. However, the spike contains trace amounts of Sr isotopes other than ^{84}Sr, which have a minor effect on the measured ratios of both $^{87}Sr/^{86}Sr$ and $^{86}Sr/^{88}Sr$, and thus on the fractionation correction. For this reason, the corrections for fractionation and for the spike contribution to $^{87}Sr/^{86}Sr$ were done offline, using an iterative routine that allows the appropriate fractionation factor for the spike-sample mixture to be calculated. As the approximate Sr concentrations were known in advance, it was possible to avoid overspiking and the large corrections and associated uncertainties on the $^{87}Sr/^{86}Sr$ ratios that would result. The mean $^{87}Sr/^{86}Sr$ for NIST SRM 987 obtained from fifty-three replicate analyses during the TIMS session of this study was 0.710242 ± 20 (2*s*). Within-run errors (2 SE) of $^{87}Sr/^{86}Sr$ were generally better than 0.00001, except for Mica-Fe (0.00005–0.0003) due to its low Sr content resulting in low intensity of the ^{86}Sr signal (≤ 0.6 V).

Rubidium measurements were performed on a Thermo Fisher Scientific Neptune Plus MC-ICP-MS at CRPG. The ^{85}Rb, ^{87}Rb and ^{88}Sr ion beams were collected on L4, L2 and L1 Faraday cups, respectively. The signal of ^{88}Sr was monitored for correction of the interference of ^{87}Sr on ^{87}Rb by assuming a constant $^{87}Sr/^{88}Sr$ ratio of 0.085. The signal of ^{88}Sr was always less than 1 mV with a $^{88}Sr/^{85}Rb$ ratio $< 2 \times 10^{-4}$. For the most radiogenic Sr sample in this study, Mica-Fe, use of the interference correction obtained assuming a $^{87}Sr/^{88}Sr$ ratio of 0.085 compared with that obtained using the measured ratio (~ 1.0 for Mica-Fe) resulted in calculated Rb contents that differed by less than 0.04%. Thus, a constant $^{87}Sr/^{88}Sr$ ratio of 0.085 was used for the interference correction for the studied samples. Each block of Rb isotope analyses consisted of 50 cycles of data with an integration time of 4.194 s per cycle. The mass bias drift was corrected by sample-standard bracketing using a 50 or 100 ppb Rb standard solutions (Plasma CAL or ASTASOL®). During the individual measurement sessions, the reproducibility of $^{87}Rb/^{85}Rb$ for the standard solutions ranged from 0.05 to 0.08% (2*s*).

3.3.3. Procedural blank contribution and correction: Rubidium and Sr blanks were determined by isotope dilution using the most diluted ^{85}Rb-enriched and ^{84}Sr-enriched spikes. A total of fifteen total chemistry blank analyses were done for nine sample digestion series, with one or two

blank measurements per series. Twelve of the Sr blanks obtained were < 2000 pg, with most being < 500 pg, but three exceptionally high blanks were found, with values of 4351 pg, 4886 pg, and 9078 pg (Figure 2). Because of the highly skewed blank distribution, use of the mean value (1641 pg) for blank correction would lead to a small but systematic bias in Sr mass fractions and isotopic ratios. For this reason, the median value of the Sr blanks (294 pg) was used. A $^{87}Sr/^{86}Sr$ ratio of 0.708 was assumed for Sr blank correction because the low ^{86}Sr signals of the blanks (always ≤ 0.16 V, with most runs < 0.01 V, Figure S1), prevented reliable analysis of their isotopic compositions. The Rb-Sr data of samples associated with the high blank with 4886 pg of Sr were rejected and are not presented here, while those run with the two other high blanks with values of 4351 pg and 9078 pg were accepted and yielded results in good agreement with those from other sessions. A second blank from the same digestion series as the 4351 pg blank was much lower (1784 pg).

The potential influence of rare high Sr blanks was evaluated by comparing the amount of Sr in the highest measured blank (9078 pg) with the Sr contents of each of the sample digestions. In the worst case, an aliquot of RM Mica-Fe containing 573 ng of Sr (Table S3), this high blank would represent 1.6% of the measured Sr. For all other reference materials, the blank contribution would be less than 1%. The effects of such contributions are shown in Table S4. For each RM, this table shows the mean Sr concentration, $^{87}Sr/^{86}Sr$, $^{87}Rb/^{86}Sr$, and the resulting age calculated assuming: 1) no blank correction; 2) the median Sr blank of 294 pg; 3) the maximum Sr blank of 9078 pg. For Mica-Fe, use of the maximum rather than the median blank would change the calculated Sr concentration by -1.4% and the $^{87}Sr/^{86}Sr$ ratio by 2.2%. For Mica-Mg, the changes would be -0.3% and 0.21%, respectively, while the effects on GL-O and FK-N would be similarly small (Table S4). These effects are smaller than the uncertainties on the mean Sr mass fractions and Sr isotope compositions representing the means of the analyses of individual digestions (Table 3). Furthermore, as the Sr blank effects on $^{87}Sr/^{86}Sr$ and $^{87}Rb/^{86}Sr$ are strongly correlated, the influence of the blank on the calculated age is negligible, ranging from 0.00% for GL-O and FK-N to 0.02% for Mica-Mg and 0.03% for Mica-Fe.

We therefore conclude that the occasional high Sr blanks obtained during our measurements had no significant effect on the results.

The total chemistry blanks for Rb were negligible. By this we mean that, after correction for the instrumental blank preceding each analysis, the $^{87}Rb/^{85}Rb$ ratios of the blanks were smaller than the $^{87}Rb/^{85}Rb$ ratio of the spikes, resulting in nonsensical calculated blank values. To place some constraints on the maximum potential Rb blank contribution, we calculated the Rb blanks using the measured $^{87}Rb/^{85}Rb$ ratios uncorrected for the instrumental contributions to ^{87}Rb and ^{85}Rb. The resulting apparent blanks, which overestimate the true total chemistry blanks, range from 526 to 1207 pg. This represents < 0.05% of the total quantity of Rb present in each sample (≥ 2495 ng Rb). Therefore, Rb blanks were negligible relative to the amounts of Rb in the samples.

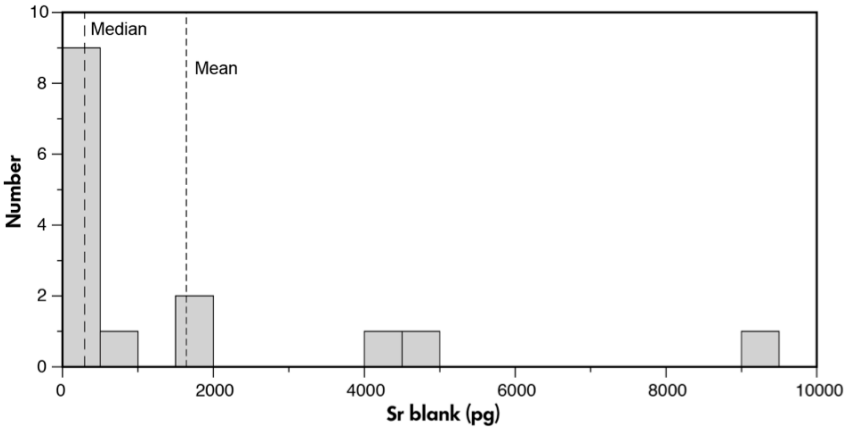

Figure 2. Frequency (number) of Sr procedural blanks during the course of this work for nine sample digestion series. Each series included one to two blanks, for a total of fifteen blanks. The difference between the median and mean values reflects the highly skewed blank distribution. Details concerning the Sr procedural blanks and their potential effects on the results are given in section 3.3.3.

3.3.4. Uncertainties on Rb-Sr ratios and mass fractions: Uncertainties for individual Sr and Rb isotope measurements are within-run errors expressed as 2 SE in Table 3, and thus represent

minimum errors on the individual measurements. The 2 SE values of $^{87}Rb/^{86}Sr$ for individual sample digestions (Table 3) were calculated using the in-run Rb and Sr mass fraction uncertainties. Additional random error sources affecting the individual analyses would include blank variability for Rb and Sr mass fractions and Sr isotope compositions, and weighing errors for the mass fractions. The latter would also affect $^{87}Rb/^{86}Sr$ ratios, as Rb and Sr spikes were added separately. Weighing uncertainties were approximately ±0.00020 g, which would correspond to uncertainties on the individual $^{87}Rb/^{86}Sr$ ratios ranging from 0.57 to 0.92%, given the quantities of spike added. As discussed in section 3.3.3, the uncertainty related to Sr blank variability is somewhat difficult to characterise, given the highly skewed blank distribution shown in Figure 2. Nevertheless, even in the worst case (Mica-Fe and highest blank) the maximum effect on the $^{87}Sr/^{86}Sr$ ratio would be ~ 2%, while the effect on the $^{87}Sr/^{86}Sr$ of the other RM would be ≤ ~ 0.2%. Adding all of these uncertainty sources together, the total maximum random errors on the individual analyses for Mica-Mg, GLO, Mica-Fe and FK-N respectively would be < 0.75%, < 1.1%, < 2.5%, and < 0.75% for $^{87}Rb/^{86}Sr$ and < 0.21%, < 0.04%, < 2.2% and < 0.20% for $^{87}Sr/^{86}Sr$.

For each RM, the mean uncertainties on Rb and Sr mass fractions and $^{87}Rb/^{86}Sr$ and $^{87}Sr/^{86}Sr$ ratios in Table 3 represent the 2*s* and 2 SE values of the means of the individual measurements. The uncertainties on the mean values automatically incorporate all of the random error components affecting each individual analysis. It is evident that the random uncertainties on the mean values for all RMs in this work are much larger than the uncertainties on the individual analyses, even if blank variability and weighing errors are included in the uncertainty on each measurement. Finally, we note that the total uncertainties (2*s*) on the mean values for each RM listed in Table 3 include not only the random components reflected in the 2*s* values, but also a systematic component reflecting the uncertainties on the spike calibration (Table 2)

Table 3a.
Rb-Sr concentrations and $^{87}Sr/^{86}Sr$ ratios of Mica-Mg for repeat analyses of the studied RMs compared with literature values.

Sample/comments	Rb (µg/g)	2 SE	2 SD	n	Sr (µg/g)	2 SE	2 SD	n	Rb/Sr	2 SD	$^{87}Rb/^{86}Sr$	2 SE	2 SD	n	$^{87}Sr/^{86}Sr$	2 SE	2 SD	n
CRPG Phlogopite Mica-Mg																		
ID-TIMS and MC-ICP-MS (this study)																		
Mica-Mg-1					27.057	0.011									1.86435	0.00001		
Mica-Mg-2					25.845	0.007									1.86493	0.00001		
Mica-Mg-3					26.334	0.009									1.86430	0.00001		
Mica-Mg-4					27.173	0.003									1.86477	0.00002		
Mica-Mg-5					26.001	0.007									1.86464	0.00003		
Mica-Mg-6	1336.8	0.1			27.528	0.003			48.6		156.34	0.02			1.86192	0.00001		
Mica-Mg-7	1329.8	0.2			27.011	0.010			49.2		158.52	0.06			1.86389	0.00001		
Mica-Mg-8	1324.4	0.2			26.451	0.002			50.1		161.22	0.03			1.86358	0.00001		
Mica-Mg-9	1302.5	0.1			27.597	0.004			47.2		151.92	0.02			1.85976	0.00001		
Mica-Mg-10[a]	1333.3	0.2			27.849	0.013			47.9		154.04	0.08			1.85558	0.00002		
Mica-Mg-10r[a]	1332.0	0.1			27.860	0.009			47.8		153.84	0.05			1.85525	0.00001		
Mica-Mg-10[a]	*1332.7*		*1.7*		*27.855*		*0.015*		*47.8*		*153.94*		*0.29*		*1.85542*		*0.00047*	
Mica-Mg-11[a]	1312.8	0.1			27.505	0.005			47.7		153.60	0.03			1.85759	0.00001		
Mica-Mg-11r[a]	1312.0	0.1			27.571	0.009			47.6		153.10	0.05			1.85468	0.00001		
Mica-Mg-11[a]	*1312.4*		*1.1*		*27.538*		*0.092*		*47.7*		*153.35*		*0.70*		*1.85614*		*0.00411*	
Mica-Mg-12[a]	1352.7	0.2			28.205	0.011			48.0		154.42	0.06			1.86329	0.00001		
Mica-Mg-12r[a]	1349.1	0.1			28.224	0.010			47.8		153.89	0.06			1.86260	0.00002		
Mica-Mg-12[a]	*1350.9*		*5.2*		*28.215*		*0.026*		*47.9*		*154.16*		*0.75*		*1.86295*		*0.00097*	
Mean[b]	**1327**	12	32	7	**27.05**	0.43	1.50	12	**49.1**	2.5	**155.6**	2.5	6.5	7	**1.8622**	0.0019	**0.0067**	12
Total uncertainty[c]			**41**				**1.51**			**2.7**			**7.3**					
ICP-MS (this study)																		
Mica-Mg	1269	28	63	18	27.19	0.75	1.68	18	47.0	3.7								
Working value																		
Govindaraju (1995)	1300		229		27		14		48.1									
Reported value by (LA)-ICP-MS/MS																		
Hogmlam *et al.* (2017)[d]											154.6		1.9		1.8525		0.0024	
Laureijs *et al.* (2021)[e]	1320		33		27		1		48.1		154.3		6.9		1.8628		0.0049	

SE: standard error, SD: standard deviation, n: the number of values included in a total mean
Each sample name by ID-TIMS and MC-ICP-MS (this study) indicates individual powder batches (50-110 mg) from different sample packets or aliquots as presented in Table S1. Mean values and their total uncertainties **in bold** are displayed in Figure 7 and 8. 2 SE values for Rb and Sr concentrations are based on in-run 2 SE uncertainties. 2 SE of $^{87}Rb/^{86}Sr$ for individual batches were calculated from error propagation of Rb and Sr concentration errors. $^{87}Sr/^{86}Sr$ uncertainties are 2 SE in-run values. See text for discussion of other potential sources of uncertainties.
[a] Duplicate analyses of each individual powder batch. The average of the duplicate values (*italic*) are included in total means.
[b] Total mean value from the replicate measurements of individual powder batches.
[c] Total uncertainty combines the random uncertainty (2 SD) of the mean of the individual analyses with the systematic uncertainty related to spike calibration (Table 2).
[d] Data by LA-ICP-MS/MS (19 analytical runs, Hogmalm *et al.* 2017). $^{87}Sr/^{86}Sr$ calibrated relative to NIST SRM 610. $^{87}Rb/^{86}Sr$ was calculated based on the calibrated $^{87}Sr/^{86}Sr$, the mean of reported ages (519.4 ± 6.5 Ma) with an assumed initial ratio (0.72607 ± 0.0007).
[e] Data by ICP-MS/MS for $^{87}Sr/^{86}Sr$ and standard addition ICP-MS for Rb and Sr concentrations of Mica-Mg powder (Laureijs *et al.* 2021).

Table 3b.
Rb-Sr concentrations and $^{87}Sr/^{86}Sr$ ratios of GL-O and FK-N for repeat analyses of the studied RMs compared with literature values.

Sample/comments	Rb (µg/g)	2 SE	2 SD	n	Sr (µg/g)	2 SE	2 SD	n	Rb/Sr	2 SD	$^{87}Rb/^{86}Sr$	2 SE	2 SD	n	$^{87}Sr/^{86}Sr$	2 SE	2 SD	n
CRPG Glauconite GL-O																		
ID-TIMS and MC-ICP-MS (this study)																		
GL-O-1	236.18	0.03			17.676	0.002			13.4		38.822	0.007			0.752872	0.00001		
GL-O-2	224.59	0.04			18.797	0.004			11.9		34.715	0.009			0.752536	0.00001		
GL-O-3	217.29	0.03			18.244	0.002			11.9		34.607	0.006			0.753228	0.00001		
GL-O-4	234.01	0.02			18.614	0.010			12.6		36.531	0.019			0.753566	0.00001		
Mean[b]	**228**	9	17	4	**18.33**	0.49	1.0	4	**12.4**	1.2	**36.2**	2.0	4.0	4	**0.75305**	0.00044	**0.00089**	4
Total uncertainty[c]			**18**				**1.0**			**1.2**			**4.0**					
ICP-MS (this study)																		
GL-O	237	5	11	18	19.11	1.02	2.3	18	12.4	1.6								
Working value																		
Govindaraju (1995)	238	5			19.3	0.5			12.3						0.7535	0.0010		
Compiled value of different laboratories from Odin et al. (1982)																		
GL-O powder[f]	239		11	5	19.2		2.2	5			36.4		5.2	5	0.7532		0.0026	5
GL-O grains[f]	239		12	15	19.3		2.1	15			36.1		4.1	15	0.7539		0.0053	15
CRPG Potash Feldspar FK-N																		
ID-TIMS and MC-ICP-MS (this study)																		
FK-N-1	814.5	0.2			36.522	0.004			22.3		67.69	0.01			1.21066	0.00002		
FK-N-2	873.9	0.1			37.149	0.023			23.5		71.41	0.05			1.21255	0.00001		
FK-N-3	870.5	0.1			37.490	0.014			23.2		70.47	0.03			1.21089	0.00001		
Mean[b]	**853**	39	67	3	**37.05**	0.57	1.0	3	**23.0**	1.9	**69.9**	2.2	3.9	3	**1.2114**	0.0012	**0.0021**	3
Total uncertainty[c]			**69**				**1.0**			**2.0**			**4.1**					
ICP-MS (this study)																		
FK-N	836	21	46	18	36.67	0.83	1.9	18	22.8	1.7								
Working value																		
Govindaraju (1995)	860		112		39		17		22.1									

SE: standard error, SD: standard deviation, n: the number of values included in a total mean
Each sample name by ID-TIMS and MC-ICP-MS (this study) indicates individual powder batches (50-110 mg) from different sample packets or aliquots as presented in Table S1. Mean values and their total uncertainties **in bold** are displayed in Figure 7 and 8. 2 SE values for Rb and Sr concentrations are based on in-run 2 SE uncertainties. 2 SE of $^{87}Rb/^{86}Sr$ for individual batches were calculated from error propagation of Rb and Sr concentration errors. $^{87}Sr/^{86}Sr$ uncertainties are 2 SE in-run values. See text for discussion of other potential sources of uncertainties.
[b] Total mean value from the replicate measurements of individual powder batches.
[c] Total uncertainty combines the random uncertainty (2 SD) of the mean of the individual analyses with the systematic uncertainty related to spike calibration (Table 2).
[f] Calculated mean value using the reported values compiled from the different laboratories by Odin *et al.* (1982).

Table 3c.

Rb-Sr concentrations and $^{87}Sr/^{86}Sr$ ratios of Mica-Fe for repeat analyses of the studied RMs compared with literature values.

Sample/comments	Rb (µg/g)	2 SE	2 SD	n[c]	Sr (µg/g)	2 SE	2 SD	n[c]	Rb/Sr	2 SD	$^{87}Rb/^{86}Sr$	2 SE	2 SD	n[c]	$^{87}Sr/^{86}Sr$	2 SE	2 SD	n[c]
CRPG Biotite Mica-Fe																		
ID-TIMS and MC-ICP-MS (this study)																		
Mica-Fe-1					6.153	0.012									8.35640	0.00007		
Mica-Fe-2					5.980	0.005									8.03423	0.00008		
Mica-Fe-3	2253.2	0.4			5.997	0.002			376		1859.9	0.8			7.97738	0.00009		
Mica-Fe-4	2219.2	0.5			5.896	0.005			376		1831.0	1.7			7.67401	0.00006		
Mica-Fe-5	2251.6	0.3			5.536	0.006			407		1987.5	2.1			7.75431	0.00005		
Mica-Fe-6	2240.2	0.1			6.384	0.002			351		1792.3	0.7			8.53462	0.00034		
Mica-Fe-7[a]	2330.4	0.6			6.491	0.004					1828.8	1.2			8.48485	0.00010		
Mica-Fe-7r[a]	2336.8	0.1			6.463	0.004					1854.0	1.1			8.60622	0.00008		
Mica-Fe-7[a]	*2333.6*		*9.0*		*6.477*		*0.039*		*360*		*1841.4*		*36*		*8.54553*		*0.17164*	
Mica-Fe-8[a]	2376.8	0.1																
Mica-Fe-8r[a]	2377.7	0.2			7.001	0.007			340		1578.8	1.6			6.91305	0.00016		
Mica-Fe-8[a]	*2377.2*		*1.3*															
Mica-Fe-9[a]	2373.0	0.2																
Mica-Fe-9r[a]	2379.0	0.2			6.550	0.006			363		1816.6	1.6			8.15958	0.00005		
Mica-Fe-9[a]	*2376.0*		*8.5*															
Mean[b]	**2293**	51	135	7	**6.22**	0.29	0.87	9	**369**	52	**1815**	92	244	7	**7.99**	0.34	**1.02**	9
Total uncertainty[c]			**142**				**0.63**			**52**			**246**					
ICP-MS (this study)																		
Mica-Fe	2174	63	141	18	5.95	0.15	0.34	18	366	32								
Working value																		
Govindaraju (1995)	2200		538		5		19		440									

SE: standard error, SD: standard deviation, n: the number of values included in a total mean

Each sample name by ID-TIMS and MC-ICP-MS (this study) indicates individual powder batches (50-110 mg) from different sample packets or aliquots as presented in Table S1. Mean values and their total uncertainties **in bold** are displayed in Figure 7 and 8. 2 SE values for Rb and Sr concentrations are based on in-run 2 SE uncertainties. 2 SE of $^{87}Rb/^{86}Sr$ for individual batches were calculated from error propagation of Rb and Sr concentration errors. $^{87}Sr/^{86}Sr$ uncertainties are 2 SE in-run values. See text for discussion of other potential sources of uncertainties.

[a] Duplicate analyses of each individual powder batch. The average of the duplicate values (*italic*) are included in total means.

[b] Total mean value from the replicate measurements of individual powder batches.

[c] Total uncertainty combines the random uncertainty (2 SD) of the mean of the individual analyses with the systematic uncertainty related to spike calibration (Table 2).

3.3.5. Reproducibilities of reference materials: For Mica-Mg and Mica-Fe, duplicate dissolutions (of 100–110 mg powder) and Rb and Sr separations were done on three individual powder batches (Mica-Mg-10, 11, 12 and Mica-Fe-7, 8, 9 in Table 3), yielding agreement within ≤ 0.27% for Rb in Mica-Mg and Mica-Fe, ≤ 0.42% for Sr in Mica-Mg and Mica-Fe, ≤ 0.16% for $^{87}Sr/^{86}Sr$ in Mica-Mg and ≤ 1.42% for $^{87}Sr/^{86}Sr$ in Mica-Fe. The mean of the duplicates was used when calculating the mean values for each RM.

Rb and Sr compositions of NIST SRM 607 K-feldspar, CRPG GA granite and CRPG BE-N basalt were determined in the same sample digestion series and analytical sessions as the other RM for quality control (Table S2). In almost all cases, the measured Rb/Sr and $^{87}Sr/^{86}Sr$ values of these secondary standards agree well within uncertainties with the literature values compiled in Table S2. For SRM-607, a difference of 2.3% was observed between our measured values and the NIST certified values for the absolute mass fractions of both Rb and Sr. However, the Rb/Sr ratio differs by

only 0.01% suggesting that a minor error in the sample weight may explain the small discrepancies in absolute Rb and Sr mass fractions for this RM. This variation could also be real, as Nebel and Mezger (2006) have documented substantial heterogeneity in this material. In addition, $^{87}Rb/^{86}Sr$ and $^{87}Sr/^{86}Sr$ ratios of SRM-607 obtained in this work are in excellent agreement with previous MC-ICP-MS results (Nebel and Mezger 2006, Waight *et al*. 2002).

Results

4.1. Imaging and chemical mapping of RM mineral grains

BSE images and elemental maps obtained by both SEM-EDS and EMPA of selected grains from Mica-Mg, GL-O, Mica-Fe and FK-N RMs are shown in Figure 3-6 and Figure S2-S5 (use of SEM-EDS or EPMA is indicated in caption to each panel). Chemical analysis of major elements by EPMA for these grains was carried out on zones devoid of impurities, inclusions or alteration to compare with the working values of bulk major element compositions proposed for the four RMs (Table S5-S8).

Phlogopite Mica-Mg: All investigated Mica-Mg grains display darker zones in BSE images that correspond to lower Fe and greater Mg contents relative to the brighter zones, as shown in the grain of Mica-Mg-j (Figure S2h). Nevertheless, Fe and Mg contents measured by EPMA in darker and brighter zones in the grain Mica-Mg-j agree within analytical error, and both agree with the working values of Govindaraju (1995) (Table S5). Compositional variability also appears in EPMA elemental maps (Figure S2a, c, d, f). The intra-grain variability of Mica-Mg grains is relatively limited for major elements (SiO_2, Al_2O_3, FeO, MgO and K_2O), as shown by the lows values of the means of the analysed EPMA points for each grain (Table S5). In the SEM-EDS elemental maps, the grains appear to have homogeneous compositions (Figure 3, S2b, e, g) due to the lower beam current (10 nA) of this technique, limiting detection of subtle compositional variations, relative to the higher beam current of 100 nA used for EPMA. The grain Mica-Mg-f display small inclusion (< 50 µm in diameter)

with higher Fe mass fractions (Figure 3). The mean Al_2O_3, FeO and MgO contents of the investigated grains ands uncertainties (% *m/m*, *n* = 22) are 14.9 ± 0.7, 7.6 ± 1.3 and 20.2 ± 1.1 respectively. One grain (Mica-Mg-a) displays FeO and MgO contents of 5.0 and 22.2 (% *m/m*), lower by 42% and higher by 9% than the working values of bulk Mica-Mg from Govindaraju (1995) (Table S5 and Figure S2a). The mean SiO_2 and K_2O contents are relatively homogenous between grains, with the mean value of each grain agreeing within uncertainty with the mean of all grains. The mean contents of Mica-Mg grains by EPMA are generally comparable to the working values of Govindaraju (1995) with a difference of less than 2% for all measured elements, except FeO, which shows a difference of 10%. If the grain Mica-Mg-a is excluded, the mean measured FeO content also agrees within error with the working value of Govindaraju (1995) (Table S5).

Glauconite GL-O: Heterogeneity in grains was observed by BSE image analysis (Figure 4a, 4b and S3). The results are consistent with a previous study by Boulesteix *et al.* (2020) who noted the presence of apatite and carbonate in GL-O grains. These authors described phosphate phases in GL-O grains as massive or disseminated apatite, as observed in the present work. Our EPMA results for apatite-free sections of GL-O grains (*n* = 12; Table S6) agree with those of Boulesteix *et al.* (2020) within theirs uncertainties, but are higher for SiO_2 by 5%, FeO by 17% and K_2O by 12% and lower for MgO by 2% and Al_2O_3 by 13%, compared with the working values of bulk GL-O from Govindaraju (1995).

Biotite Mica-Fe: BSE images and elemental maps of Mica-Fe grains show that grains include variable types of mineral inclusions such as apatite, monazite, K-feldspar, zircon and ilmenite (Figure 4c, 4d, 5, S4d and S4e). Mica-Fe grains display compositional variation at the intra-grain scale with relative uncertainties (SD) up to 1.7% for SiO_2, 3.8% for Al_2O_3, 4.5% for FeO, 3.2% for MgO and 2.5% for K_2O, respectively (Table S7). Compositional variability of Mica-Fe in randomly selected grains was relatively low compared with that of Mica-Mg grains, with the mean ands (% *m/m*, *n* = 17) of 34.6 ± 0.4 for SiO_2, 18.9 ± 0.4 for Al_2O_3, 22.9 ± 0.6 for FeO, 4.7 ± 0.2 for MgO, 9.0 ± 0.1 for K_2O

and 2.4 ± 0.1 for TiO_2. The mean values of EPMA results are in good agreement with the working values of bulk Mica-Fe from Govindaraju (1995) within its uncertainty limits (1*s*).

Potassium feldspar FK-N: BSE images and elemental maps show that all investigated FK-N grains do not occur as pure single varieties but as a perthite containing sodium feldspar in various proportions with small inclusions of quartz (Figure 6 and S5), consistent with the reported sample description in Govindaraju (1984). EPMA analyses were done on the perthite and the anti-perthite phases of the grains resulting in a high deviation of the EPMA results of the FK-N grains compared with the working values of Govindaraju (1995) for bulk FK-N. The mean Na_2O and K_2O contents (n = 19) are 1.7 times higher in Na_2O and 0.8 times lower in K_2O than the working values of Govindaraju (1995) (Table S8). The mean orthoclase (Or) contents of potassium feldspar sections (n = 13) in FK-N grains measured by EPMA is 88 mol.% and the reported Or content of bulk FK-N from Govindaraju (1984) is 77 mol.%. The difference of 13% in the Or contents between the bulk FK-N from of Govindaraju (1984) and potassium feldspar sections in FK-N grains in our study indicates that the Or content is highly variable at the intra-grain scale, and that a small number of grains will not be representative of the bulk FK-N RM.

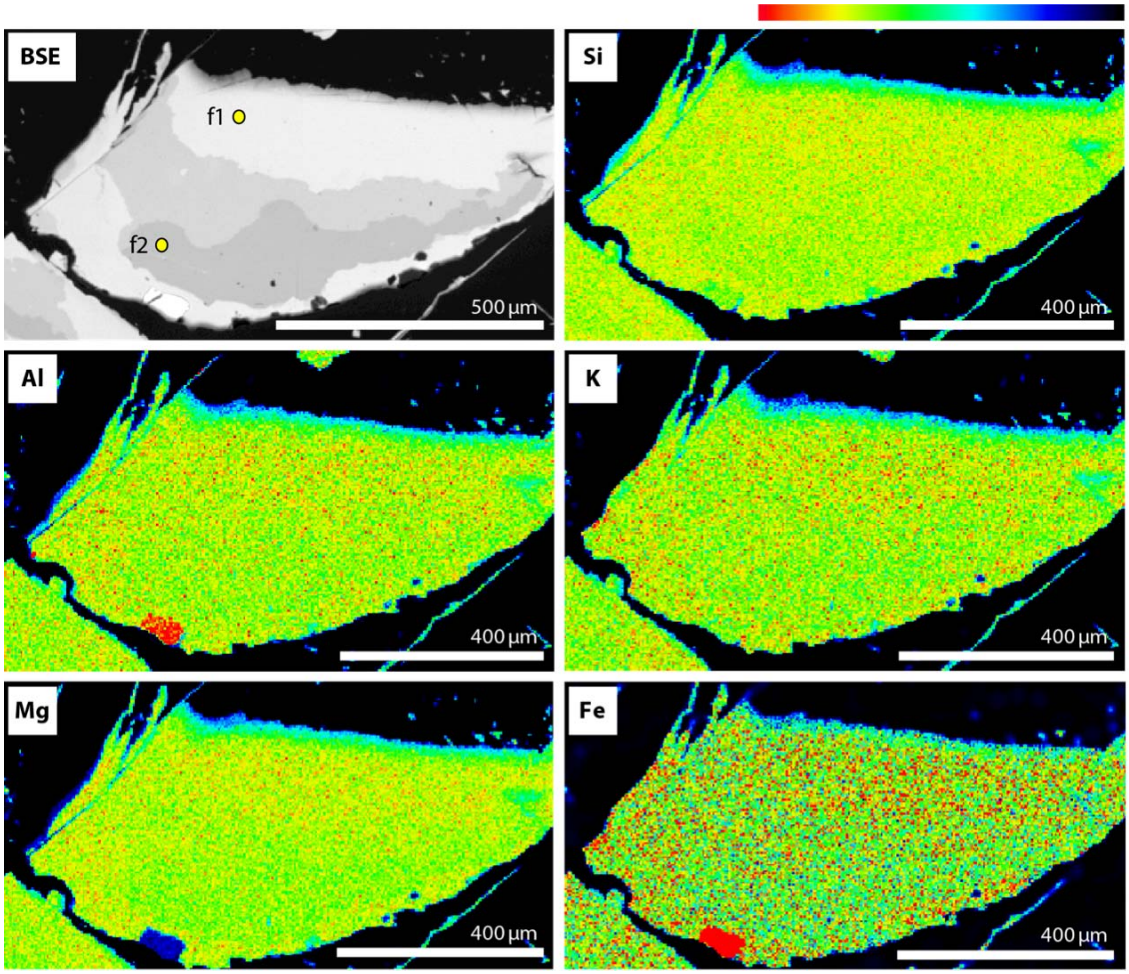

Figure 3. BSE image and SEM-EDS elemental maps of a grain of Mica-Mg phlogopite (Mica-Mg-f). The coloured scale bar on the top shows the relative abundance of the mapped major element scaled between 0 (dark blue) and 100 (red). The elemental maps show a small area with higher Fe and lower Mg within the grain. Yellow circles indicate spot locations of EPMA in Table S5.

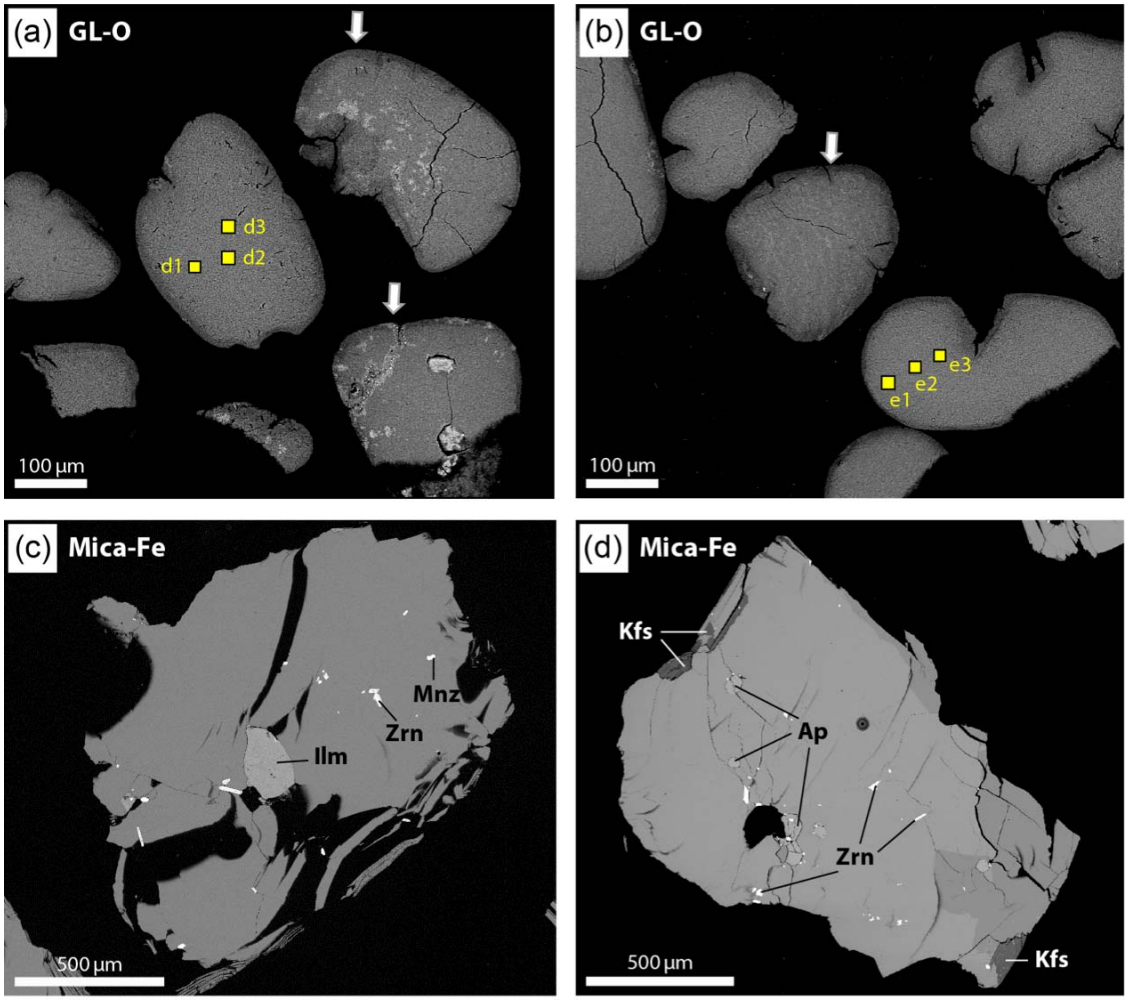

Figure 4. BSE images displaying heterogeneity of (a, b) GL-O glauconite grains and (c, d) Mica-Fe biotite grains. Heterogeneous grains in (a) and (b) are indicated by arrows. Lighter sections in the grains correspond to phosphate minerals (apatite) as previously observed by Boulesteix *et al.* (2019). Yellow square points represent locations of 10 x 10 µm defocused analyses by EPMA of the GL-O grains (Table S6). (c) and (d) show various mineral phases including ilmenite (Ilm), zircon (Zrn), monazite (Mnz), apatite (Ap) and K-feldspar (Kfs) within Mica-Fe grains.

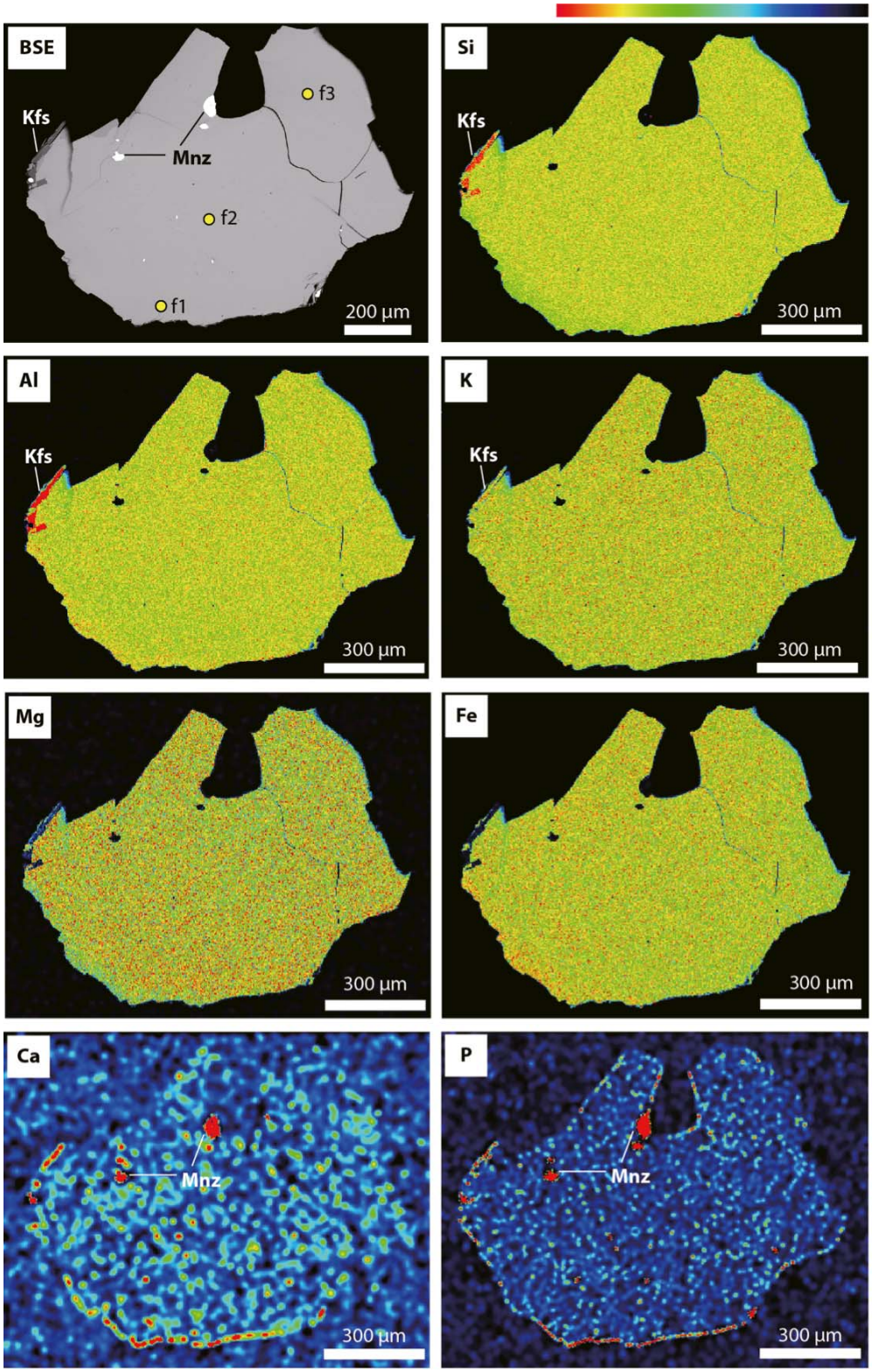

Figure 5. BSE image and SEM-EDS elemental maps for a grain of Mica-Fe biotite (Mica-Fe-f), showing heterogeneities including K-feldspar (Kfs) and monazite (Mnz). Explanation of coloured scale bar given in Figure 3 caption. Yellow circles indicate spot locations of EPMA in Table S7.

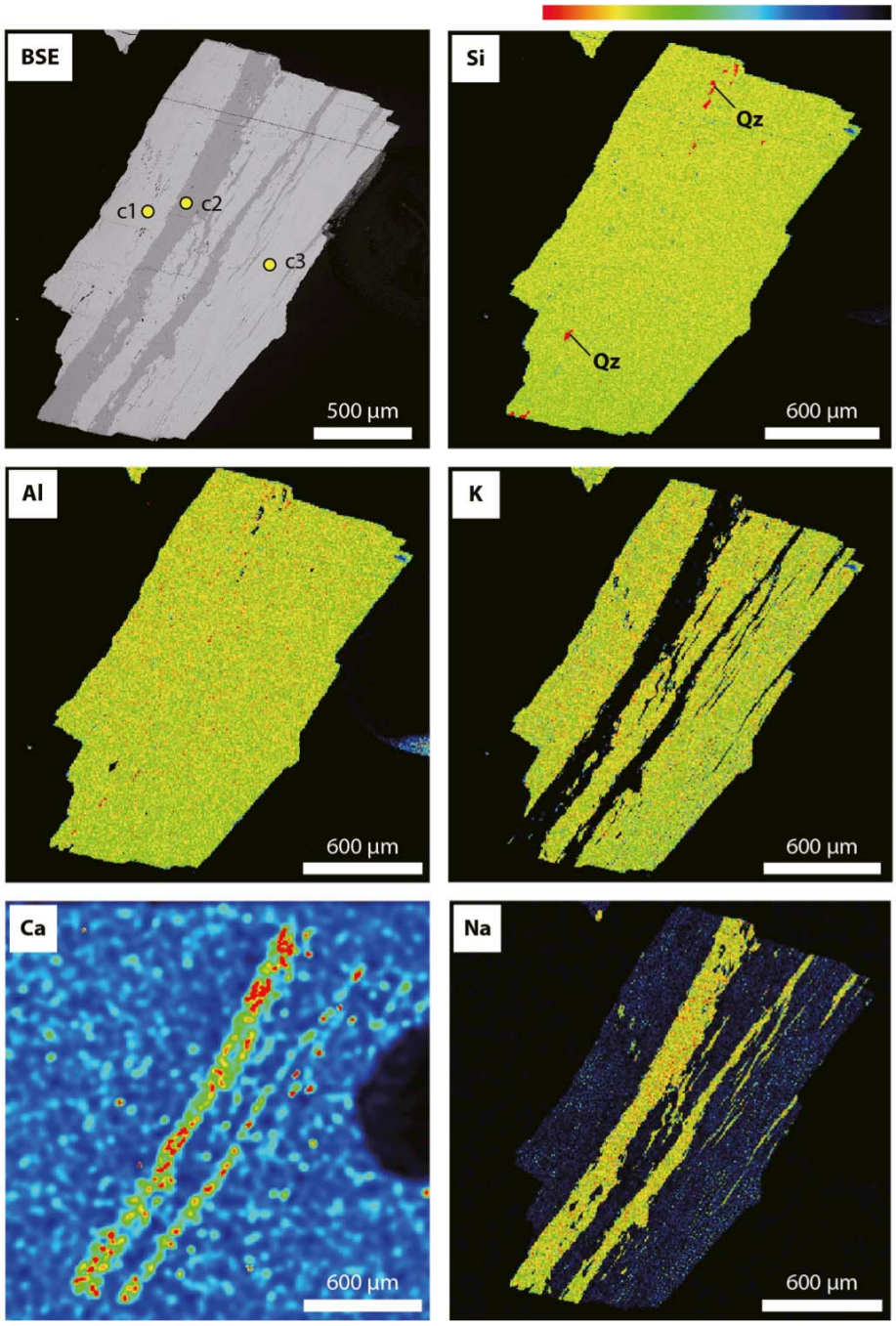

Figure 6. BSE image and SEM-EDS elemental maps for a grain of FK-N potassium feldspar (FK-N-c), displaying the coexistence of orthoclase and albite (Ca- and Na-rich zones) and small inclusions of quartz (Qz). Explanation of coloured scale bar given in Figure 3 caption. Yellow circles indicate spot location of EPMA in Table S8.

4.2. Bulk powder Rb and Sr mass fractions and isotope compositions of the four RMs

Rubidium and Sr mass fractions and Rb-Sr isotopic compositions obtained for the four RMs are given in Table 3 and 4 and shown in Figure 7 and 8. Multiple measurements of individual powder batches from different bags or aliquots were performed for the four RMs (Table S1). The means of the multiple analyses and their standard error (2 SE) and standard deviation (2*s*) are presented in Table 3 and were used to evaluate the compositional homogeneity of the bulk samples. As discussed in section 3.3.4, the uncertainties of the total mean values indicate random errors from multiple measurements of different powder batches, which include the uncertainties from the Sr blank contribution.

Rubidium and Sr contents obtained by the isotope dilution method using TIMS and MC-ICP-MS and by the alkali fusion method using ICP-MS are presented in Figure 7, Table 3 (TIMS and MC-ICP-MS) and Table S9 (ICP-Q-MS). The mean Rb and Sr mass fractions of the four RMs measured by the two methods were within uncertainty of the working values of Govindaraju (1995). This is also true of the Rb and Sr contents of the individual batches (Figure 7). Differences < 1.0% were observed in the mean Rb/Sr ratios of Mica-Fe, GL-O and FK-N between the two methods (Table 3). A difference of 4.8% in the mean Rb/Sr ratios for Mica-Mg between the two methods was obtained, but they overlap well within 2*s* uncertainties. The means from 18 analyses of different powder aliquots for the Rb/Sr concentration ratios by alkali fusion ICP-MS have uncertainties (2*s*, n = 18) of 7.9% for Mica-Mg, 13% for GL-O, 8.7% for Mica-Fe and 7.5% for FK-N, respectively. The mean Rb/Sr concentration ratios of multiple measurements by ID-TIMS and ID-MC-ICP-MS yield mean and total uncertainties (2*s*) of 5.1% and 5.5% for Mica-Mg (n = 7), 9.4% and 9.6% for GL-O (n = 4), 14.1% and 14.2% for Mica-Fe (n = 7) and 8.3% and 8.5% for FK- N (n = 3), respectively.

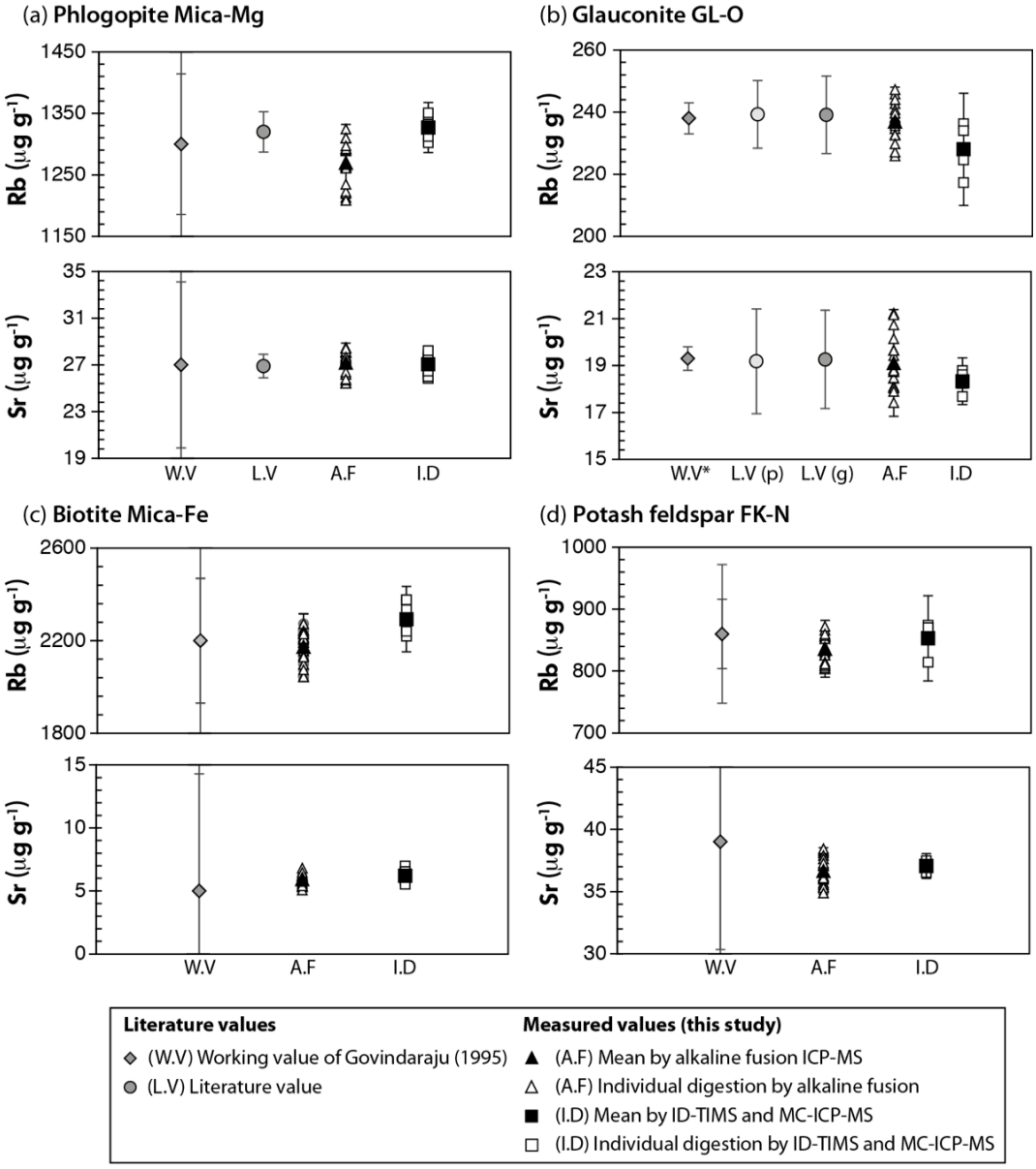

Figure 7. Comparison of Rb and Sr mass fractions determined by alkali fusion ICP-MS and ID-TIMS and ID-MC-ICP-MS, and with literature values. Uncertainties (2*s*) for the measurements by alkali fusion ICP-MS are shown for the mean values. Error bars for the mean values by ID-TIMS and ID-MC-ICP-MS correspond to the total uncertainties (2*s*) in Table 3 and are smaller than the spread of the symbols for the individual Sr contents of Mica-Mg and Mica-Fe. Error bars from working values (W.V) of Govindaraju (1995) indicate ± 1*s* and 2*s*, except for GL-O for which the bars indicate 95% confidence limits (W.V*) given by Govindaraju (1995). Literature values (L.V) are from (a) Laureijs *et al.* (2021) and (b) compiled data of different laboratories from Odin *et al.* (1982) for powder (p) and grains (g) of GL-O. Details of the literature data are provided in Table 3.

The Rb/Sr and Sr isotope compositions obtained for the four RMs are given in Table 3 and 4 and shown in Figure 8. The mean $^{87}Rb/^{86}Sr$ ratio for Mica-Mg (n = 7) is 155.6 with mean and total errors (2*s*) of 4.2% and 4.7%, respectively. The mean $^{87}Sr/^{86}Sr$ ratio for Mica-Mg (n = 12) is 1.8622 with a mean error (2*s*) of 0.36%. The measured Rb/Sr and Sr isotopic values agree with the literature data within their reported uncertainties (Hogmalm *et al.* 2017, Laureijs *et al.* 2021). GL-O was measured on four different batches, yielding a mean $^{87}Rb/^{86}Sr$ ratio of 36.2 with mean and total uncertainties (2*s*) of 10.9% and 11.1%, respectively. The mean of $^{87}Sr/^{86}Sr$ ratios is 0.75305 with a mean uncertainty (2*s*) of 0.12%. The compositional variability of Rb/Sr and Sr isotopic compositions of GL-O is very similar to the variation of the literature values on GL-O grains and powder from Odin *et al*. (1982). To our knowledge, there are no literature data for Sr isotope compositions for Mica-Fe and FK-N. The mean $^{87}Rb/^{86}Sr$ ratio for Mica-Fe (n = 7) is 1815 with an mean and total uncertainties (2*s*) of 13.4% and 13.6%, respectively. The mean $^{87}Sr/^{86}Sr$ ratio for Mica-Fe (n = 9) is 7.99 with a mean uncertainty of 13%. The mean $^{87}Rb/^{86}Sr$ ratio for FK-N (n = 3) is 69.9 with 2*s* of 5.6% and 5.9% for mean and total uncertainties, respectively. The mean $^{87}Sr/^{86}Sr$ ratio for FK-N (n = 3) is 1.2114 with a mean uncertainty (2*s*) of 0.17%.

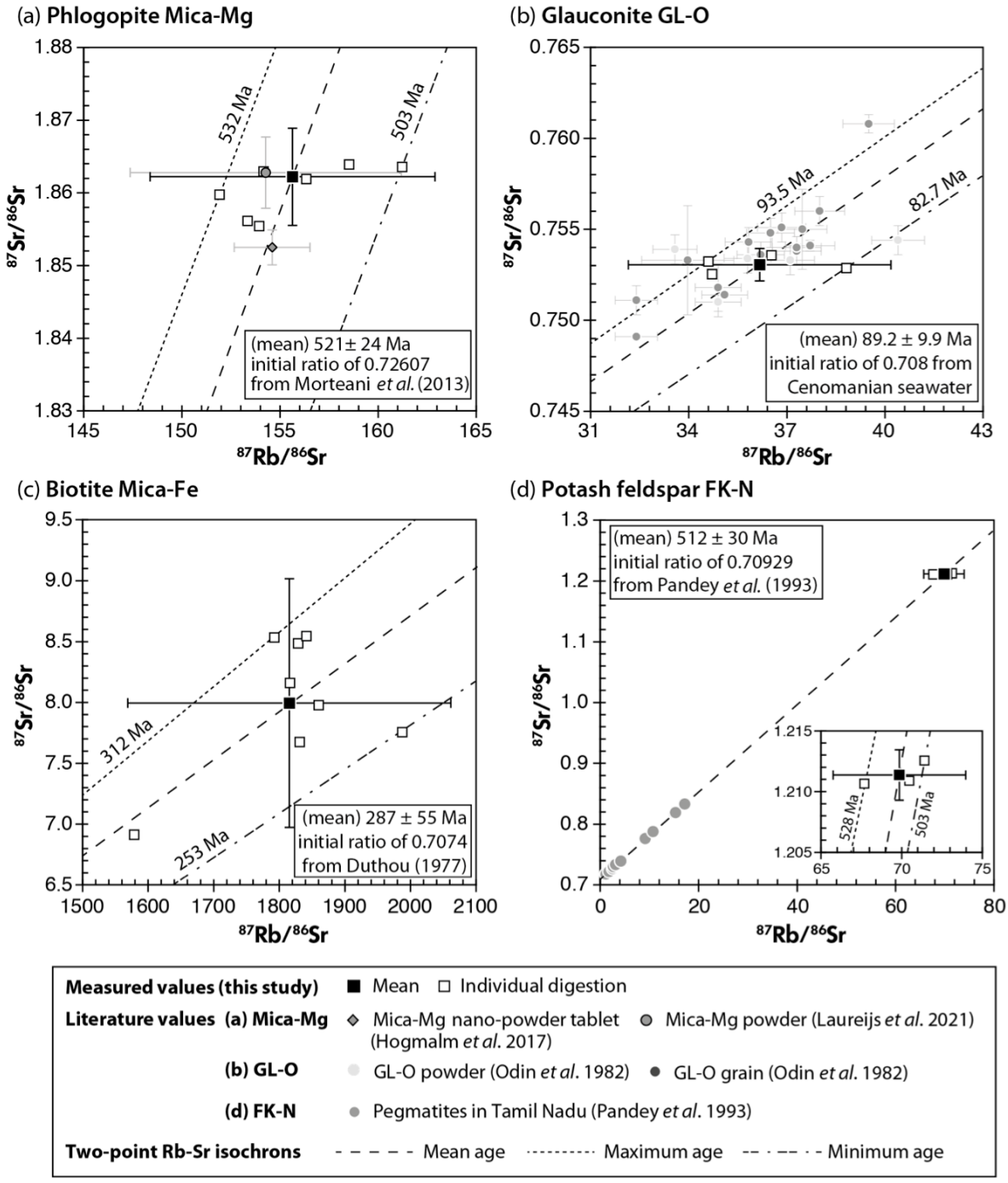

Figure 8. Measured $^{87}Rb/^{86}Sr$ and $^{87}Sr/^{86}Sr$ isotope compositions, compiled with literature data, for (a) Mica-Mg, (b) GL-O, (c) Mica-Fe and (d) FK-N. Errors in the mean $^{87}Rb/^{86}Sr$ and $^{87}Sr/^{86}Sr$ ratios are total uncertainties (2*s*) in Table 3. Uncertainties (2 SE) for the individual digestions are smaller than the symbols for $^{87}Sr/^{86}Sr$ and $^{87}Rb/^{86}Sr$. Dotted lines in (a), (b), (c) and (d) indicate 2-point isochrons using the mean and individual values analysed in this study and assumed initial ratios (see text for details). Isochron age uncertainties were calculated using maximum likelihood regressions

implemented in the online version of IsoplotR (Vermeesch 2018, http://isoplotr.es.ucl.ac.uk/). (d) Errors in $^{87}Rb/^{86}Sr$ and $^{87}Sr/^{86}Sr$ ratios from Pandey *et al.* (1993) are 2% and 0.05%, respectively. Literature data and their errors are given in Table 3.

Table 4.
Working values and uncertainties for the RMs in this study

Sample	**$^{87}Rb/^{86}Sr$**	**2 SD**	**$^{87}Sr/^{86}Sr$**	**2 SD**
Phlogopite Mica-Mg	155.6	7.3 (4.7%)	1.8622	0.0067 (0.36%)
Glauconite GL-O	36.2	4.0 (11%)	0.75305	0.00089 (0.12%)
Biotite Mica-Fe	1815	246 (14%)	7.99	1.02 (13%)
Potassium Feldspar FK-N	69.9	4.1 (5.9%)	1.2114	0.0021 (0.17%)

Uncertainties on the $^{87}Rb/^{86}Sr$ values include both random component from replicate analyses and systematic component related to spike calibration.

Discussion

Three different aspects are considered to evaluate the suitability of the Mica-Mg, Mica-Fe, GL-O and FK-N RMs as potential reference materials for *in situ* Rb-Sr dating by LA-ICP-MS/MS. The first is the possible effect of chemical and mineralogical heterogeneities, both within individual mineral grains and between grains, on the bulk Rb/Sr and Sr isotopic values of the RMs. The second is the precision of the determined Rb/Sr and Sr isotope compositions and their uncertainties. The third is the comparison between the absolute ages for the four RMs that can be inferred from our data with previously suggested ages for these RMs.

5.1. Homogeneity of the RMs at the scale of mineral grains

At the grain scale, BSE images, elemental maps and EPMA analyses (Figure 3-6, Table S5-S8, Figure S2-S5) of the four RMs show varying degrees of heterogeneity in their major element compositions.

The geological contexts of the RM are considered in order to better understand the origin of this heterogeneity.

Phlogopite Mica-Mg was separated from a pyroxenite in the Bekily area, southern Madagascar (Govindaraju 1979). The location of the pyroxenite and name of the sampled zone are not given and a recent search of the available documentation at the SARM unfortunately did not provide additional information. In BSE images and SEM-EDS and EPMA elemental maps of selected grains, the intra-grain compositions of Mica-Mg show only limited heterogeneity evident as small areas with high Fe contents in a few grains (Figure 3 and S2). As noted above, only one grain (Mica-Mg-a, Table S5) displays significantly lower FeO and higher MgO contents than other grains and the working value of Govindaraju (1979). Govindaraju (1979) reported that the initial form of Mica-Mg was large sheets without any visible impurities. This may explain our observation that the compositional variation is small. The limited extent of heterogeneity is confirmed by the consistency of the measured Rb and Sr contents by alkali fusion ICP-MS and ID-TIMS and MC-ICP-MS and their agreement with the working values of bulk Mica-Mg from Govindaraju (1979). Phlogopites from Ampandarandava and nearby deposits in southern Madagascar, occurring in a matrix of calcite, anhydrite and diopside, have been reported to have homogeneous major element compositions (Martin *et al.* 2014, Morteani *et al.* 2013). Nevertheless, the presence of micro-inclusions of titanite and rutile, inclusions of calcite or anhydrite was documented in these phlogopites (Martin *et al*. 2014). Such inclusions were not observed within the tested Mica-Mg grains in our study.

For glauconite GL-O, no impurities were detected under microscopic observation in early work (Odin *et al*. 1982), but the recent study of Boulesteix *et al*. (2020) revealed the presence of included microphases such as apatite and calcite. Their observation is in good agreement with our BSE imaging results (Figure 4a, 4b and S3). EPMA results on GL-O grains show a high discrepancy of the major element contents compared with the working values of Govindaraju (1995), consistent with the findings of Boulesteix *et al*. (2020). These authors suggested that the discrepancy between the major

element composition of GL-O powder and the grains analysed *in situ* reflected the contribution of the phosphate inclusions in GL-O. If the bulk compositions of GL-O are highly impacted by impurities such as apatite, the Rb/Sr ratios could also be biased compared with phosphate-free GL-O grains.

Biotite Mica-Fe was separated from a biotite emplaced in a magmatic shear zone within the Saint-Sylvestre two mica leucogranitic complex near Razès, France (Friedrich 1983, Govindaraju 1979). This complex is dominated by a two-mica granite (granite de Saint-Sylvestre) composed of quartz ± Fe biotite ± muscovite ± plagioclase ± K-feldspar ± sillimanite (Cuney *et al.* 1990, Turpin *et al.* 1990, Villaros and Pichavant 2019). The sampled biotite corresponds to the latest phase of crystallisation of magma expelled from the Fanay fine grained peraluminous leucogranite intrusion in the Saint-Sylvestre leucogranitic complex (Friedrich 1983, Friedrich *et al.* 1987). This magma was very rich in incompatible elements (e.g., U, Th, REE, K, Zr, Rb), explaining the high proportion of minerals bearing these elements (monazite, zircon, apatite) included within biotite grains (Figure 4c, 4d, 5 and S4), as well as the high Rb/Sr ratio and highly radiogenic Sr composition measured for Mica-Fe. Inclusions of apatite, monazite, K-feldspar, zircon and ilmenite in Mica-Fe are depleted in Rb and/or Sr compared with biotite and therefore could affect the bulk Rb-Sr isotope compositions of the Mica-Fe bulk sample if their proportion varies between aliquots. Such impurities in Mica-Fe grains were reported during separation of Mica-Fe by Govindaraju (1979), with 13 kg of minerals including muscovite, quartz and feldspars being eliminated. Reported Rb and Sr mass fractions of biotite flakes extracted from the Saint-Sylvestre granite by Duthou (1977) are 2660 ppm and 4.1 ppm (sample B1354) and 1335 ppm and 5.2 ppm (sample B1355), respectively, and the reported values for $^{87}Rb/^{86}Sr$ and $^{87}Sr/^{86}Sr$ isotopic ratios are 1884 ± 54 and 8.69 ± 0.09 (sample B1354) and 739 ± 22 and 3.94 ± 0.04 (sample B1355), respectively. The latter value is significantly less radiogenic than those we measured for Mica-Fe. Together, the Duthou (1977) values define two-point isochrons of 303 ± 9 Ma for sample B1354 and 312 ± 10 Ma for sample B1355 using the initial $^{87}Sr/^{86}Sr$ ratio from Duthou (1977) (see Figure S6 for further details). These previous results are consistent with the highly radiogenic and quite variable composition of Mica-Fe obtained in the present study (7.99 ± 13% (2*s*)

for $^{87}Sr/^{86}Sr$ and 1815 ± 14% (2*s*) for $^{87}Rb/^{86}Sr$). Newly reported Rb/Sr mass fraction ratios of biotite from a sample from the Saint-Sylvestre granite range from 59 to 640 (Villaros and Pichavant 2019), further supporting the variability observed in our Mica-Fe samples.

Potassium feldspar FK-N originates from Tamil Nadu, India (Govindaraju 1984), where orthoclase-rich and quartz-rich leucocratic medium grained to pegmatitic granites and pink coarse to pegmatitic granites occur (Roy and Raju 1999). Feldspars from pegmatitic rocks in the Tamil Nadu area occur as K-feldspar composed of microcline mixed with various proportions of sodic plagioclase intergrown as perthite (Roy and Raju 1999). The reported mineralogy of feldspars from pegmatitic rocks in Tamil Nadu is consistent with our EPMA results and elemental maps (Figure 6 and S4, Table S8) and the sample description of FK-N given in Govindaraju (1984). Highly variable Rb/Sr mass fraction ratios with ranges of 7.5% (2*s*, n = 18) and 8.5% (2*s*, n = 3) were measured by alkali fusion ICP-MS and ID-TIMS and MC-ICP-MS, respectively. The heterogeneity of FK-N grains, observed from our microscopic and SEM-EDS observations and EPMA results, potentially affects the bulk composition of FK-N, likely explaining the high variability of trace element characteristics such as Rb/Sr ratios.

Our study of the four RMs at the grain scale combined with previous work shows that these RMs display differing degrees of chemical and mineralogical heterogeneities. GL-O, Mica-Fe and FK-N present the most heterogeneity, as observed in the variability of the chemical analyses, whereas Mica-Mg is somewhat more homogeneous.

5.2. $^{87}Sr/^{86}Sr$ and Rb/Sr ratio determinations and homogeneity of RMs

Rb-Sr analyses for each RM, obtained from separate aliquots of multiple powder batches provided by the SARM, show variable spread in $^{87}Sr/^{86}Sr$ compositions and Rb/Sr mass fraction ratios as shown in Figures 7 and 8, implying heterogeneity in the bulk powder samples. The degree of heterogeneity is not equivalent between the RMs, as can be seen by comparing the uncertainties on their mean Rb-Sr mass fractions and isotopic ratios obtained by ID-TIMS and ID-MC-ICP-MS (Table 3). These

uncertainties values reflect both random measurement errors, including variable Sr blank contributions (Table S4) and potential powder heterogeneity both within and between different batches of each RM, and systematic uncertainties related to the spike calibration (Table 2).

Measurements of Rb and Sr mass fractions were done using two methods (Alkali fusion ICP-MS and ID-TIMS + MC-ICP-MS) to test the validity of the analytical protocols and the homogeneity of the RMs. The coherent and reproducible results of Rb/Sr ratios acquired using the two methods on multiple batches of the RMs taken from different bags argues for the reliability of both methods. The large ranges in the Rb/Sr mass fraction ratios measured for the four RMs, with mean uncertainties (2*s*) of 7.5–13% and 5.1–14% determined respectively by the alkali fusion and the isotope dilution methods, imply sample heterogeneity in Rb-Sr compositions exceeding the analytical errors.

The analyses of seven individual digestions for Mica-Mg yielded a mean $^{87}Rb/^{86}Sr$ ratio of 155.6 ± 7.3 (4.7%, 2*s*) (Table 3a). This value is identical within error to the calculated $^{87}Rb/^{86}Sr$ ratio of 154.6 ± 1.2% for nano-powder pellet Mica-Mg obtained by Hogmalm *et al*. (2017) and the measured $^{87}Rb/^{86}Sr$ ratio value of 154.3 ± 4.5% for powder Mica-Mg given by Laureijs *et al*. (2021). In addition to random measurement related uncertainties, the uncertainties of our measured and literature data for Rb/Sr mass fraction and isotopic ratios of Mica-Mg are considered to reflect minor compositional heterogeneities between different aliquots of the Mica-Mg bulk sample. Our data on Mica-Mg do not reflect the high variability of Rb/Sr ratios on intra-grain and grain-to-grain scales previously reported for phlogopite minerals from deposits in the Bekily area (Morteani *et al.* 2013).

The mean $^{87}Rb/^{86}Sr$ value from analyses (Table 3b) of four individual digestions of GL-O is 36.2 ± 4.0 (11%, 2*s*). Odin *et al*. (1982) reported results of an interlaboratory comparison of Rb-Sr isotopic analyses of GL-O powder, showing large scatter in both Rb/Sr mass fractions and $^{87}Sr/^{86}Sr$ (Figure 7b and 8b). The mean $^{87}Rb/^{86}Sr$ value of the GL-O powder from the Odin *et al*. (1982) compilation is 36.4 ± 14% (2*s*, n = 5) in excellent agreement with our results (Table 3b). Their study also presented

compiled interlaboratory results for GL-O grains, which yielded a mean $^{87}Rb/^{86}Sr$ value of 36.1 ± 11% (2*s*, n = 15). These large uncertainties could reflect procedural differences between laboratories and/or heterogeneity between the different GL-O powder batches. The latter possibility is supported by BSE imaging and EPMA results for GL-O grains showing phosphate inclusions and within grain major element variations. The mean major element contents of inclusion-free sections of GL-O grains in our study differed from the working values of bulk GL-O given by Govindaraju (1995). These results indicate that GL-O is affected by impurities and chemical variations on both an inter and intra-grain scale, which affect Rb and Sr mass fractions and isotope compositions of the bulk sample powder.

The mean of $^{87}Rb/^{86}Sr$ ratios from seven individual digestions of Mica-Fe is 1815 ± 246 (14%, 2*s*) (Table 3c). We consider that bulk Mica-Fe is heterogeneous, so different powder aliquots may have contained different proportions of mineral inclusions with $^{87}Sr/^{86}Sr$ and Rb/Sr ratios distinct from those of the biotite. In addition to Rb/Sr isotopic heterogeneity introduced from inclusions, the large spread in Rb/Sr and Sr isotope compositions of Mica-Fe may be due to high and variable Rb/Sr ratios within biotite (Villaros and Pichavant 2019), which over time produced highly radiogenic and variable $^{87}Sr/^{86}Sr$ compositions in the biotitite from which Mica-Fe was extracted (Friedrich 1983). Interaction with post-crystallisation fluids in the Saint-Sylvestre complex associated with the formation of uranium deposits (Turpin *et al.* 1990), may have led to a heterogeneous distribution of the Rb/Sr isotopic ratios at the grain and/or the bulk sample scale (discussed below).

Three analyses of $^{87}Rb/^{86}Sr$ ratios for FK-N yielded a mean value of 69.9 ± 4.1 (5.9%, 2*s*) (Table 3b). Chemical heterogeneity within and between grains of FK-N was observed in EPMA measurements with varying major element contents and discrepancies relative to the working value of bulk FK-N from Govindaraju (1995). This variability within and between FK-N grains suggests that Rb/Sr isotopic heterogeneity of the bulk powder could be derived from variable amounts of potassium feldspar and sodium plagioclase in different aliquots.

To summarise, the analyses done on multiple powder digestions of the four tested RMs show variable degrees of dispersion in Rb and Sr mass fractions and $^{87}Rb/^{86}Sr$ ratios. Such dispersion is consistent with observations done by SEM and EPMA and with the findings of previous studies. The most heterogeneous RMs are Mica-Fe and GL-O for Rb/Sr values with total uncertainties of 14% and 11% (2*s*), respectively, and the most reproducible Rb/Sr values were obtained for Mica-Mg with a total uncertainty of 4.7% (2*s*) followed by FK-N with an uncertainty of 5.9% (2*s*). We consider that the $^{87}Rb/^{86}Sr$ heterogeneity measured in the bulk RMs is derived mainly from the initial heterogeneity of their original crystals. The addition of the spike to the sample resulted in additional uncertainties linked to the spike calibration. Based on these considerations, we propose our working values of $^{87}Rb/^{86}Sr$ and $^{87}Sr/^{86}Sr$ ratios for the RMs with their total uncertainties in Table 4.

5.3. Model ages of the RMs

Rb-Sr model ages of the RMs calculated from the mean Rb-Sr isotopic values obtained by ID-TIMS and ID-MC-ICP-MS and the total uncertainties (2*s*) are presented in Table 1 and the associated two-point isochrons are shown in Figure 8. All model ages are calculated using maximum likelihood regressions in Isoplot R (Vermeesch 2018, http://isoplotr.es.ucl.ac.uk/) with $\lambda^{87}Rb = 1.3972 \pm 0.0045 \times 10^{-11}$ a, an estimate of initial $^{87}Sr/^{86}Sr$ ratio and uncertainties are reported at 95% confidence.

A two-point isochron age of 521 ± 24 Ma of Mica-Mg using the mean $^{87}Rb/^{86}Sr$ and $^{87}Sr/^{86}Sr$ ratios (Figure 8a) is obtained assuming an initial $^{87}Sr/^{86}Sr$ of 0.72607, also assumed by Hogmalm *et al.* (2017). This value was constrained by Morteani *et al.* (2013) from two diopside samples paired with two phlogopite samples from the Ampandrandava deposit. This calculated age is in agreement with previous age determinations on Mica-Mg within reported uncertainties (Govindaraju 1979, Laureijs *et al.* 2021, Zimmermann *et al.* 1985). The individual two-point isochron ages range from 503 to 532 Ma using the measured Rb-Sr isotopic ratios of individual digestions of Mica-Mg (Figure 8a). This result is also coherent with other local geochronological dates from the Bekily area of southern Madagascar, such as Rb-Sr phlogopite ages of 518 ± 8 Ma (Morteani *et al.* 2013) and 500 ± 10 Ma

(Martin *et al.* 2014), re-calculated using the ^{87}Rb decay constant of Villa *et al*. (2015), and a U-Pb zircon age of 526 ± 34 Ma (Kröner *et al.* 1996).

The mean ^{87}Rb/^{86}Sr and ^{87}Sr/^{86}Sr ratios for GL-O yield a two-point isochron age of 89.2 ± 9.9 Ma with a range of 82.7 to 93.5 Ma for the individual digestions (Figure 8b) using the estimated initial ^{87}Sr/^{86}Sr ratio of 0.708 for Cenomanian seawater, reported in Odin *et al*. (1982). This calculated age is within the range of the reported Rb-Sr and K-Ar ages for original GL-O powder and grains compiled in Table 1 (Odin *et al*. 1982, Smith *et al*. 1998). The large variation in reported ages and our calculated ages and uncertainties reflect sample heterogeneity in the bulk sample of GL-O, as GL-O grains shows compositional zones and have mineral impurities including apatite and calcite.

A two-point isochron age of 287 ± 55 Ma for Mica-Fe was calculated using the mean Rb/Sr and Sr isotope compositions of Mica-Fe, with a range of 253 to 312 Ma for the individual digestions (Figure 8c). Individual ^{87}Sr/^{86}Sr ratios are scattered and not linearly correlated with ^{87}Rb/^{86}Sr, resulting in the high uncertainty on the age. Though there is some overlap within uncertainty, our calculated ages for Mica-Fe are younger than previously determined ages for this RM obtained by Rb-Sr, K-Ar and Ar-Ar dating (Govindaraju 1979, Grove and Harrison 1996, Zimmermann *et al.* 1985). They are also younger than ages for the Saint-Sylvestre leucogranite that encloses the biotitites, which include Ar-Ar plateau ages obtained on muscovites (302.1 ± 0.87 Ma) and biotite (302.44 ± 0.63 Ma and 301.44 ± 0.65 Ma) (Scaillet *et al.* 1996), U-Pb zircon and monazite ages of 324 ± 4 Ma (Holliger *et al.* 1986) and a whole-rock Rb-Sr isochron age of 320 ± 18 Ma (Duthou 1977, age recalculated using the revised ^{87}Rb decay constant of Villa *et al.* 2015). In our calculations, an initial ^{87}Sr/^{86}Sr ratio of 0.7074 was used, derived from the whole-rock Rb-Sr isochron of the Saint-Sylvestre leucogranite reported in Duthou (1977). To test whether the variability of our calculated ages and the bias relative to previous ages could be caused by the choice of initial ratio, we recalculated our ages assuming initial ^{87}Sr/^{86}Sr between 0.7039 and 0.7130 corresponding to the range of initial ratios of individual granite samples from Duthou (1977) calculated using the U-Pb zircon and monazite ages of 324 ± 4 Ma (Holliger *et al*.

1986). This variation of initial ratios modifies the calculated ages by only 0.04-0.09% (Figure 9), implying that other factors are responsible for the large variation and bias in our results. Mica-Fe has an exceptionally high Rb/Sr ratio (2293 µg g^{-1} of Rb for only 6.2 µg g^{-1} of Sr), coupled with an extremely radiogenic Sr composition (Friedrich *et al.* 1987, Govindaraju 1979). This implies that even minor changes in Rb or Sr abundances occurring since the biotite formed could inordinately affect the calculated age. Mica-Fe grains are quite heterogeneous, with abundant inclusions of apatite, monazite, zircon, K-feldspar and ilmenite with different Rb/Sr ratios. While such grains should in theory not affect the calculated age if they were included within and equilibrated with the biotite at the time it formed, they could instead provide evidence of alteration of the system. Turpin *et al*. (1990) reported that alteration of the Saint-Sylvestre complex by oxidised hydrothermal fluids continued for 25 Ma after granite emplacement, as dated from barren episyenites at 306 ± 2 Ma (recalculated using the ^{87}Rb decay constant of Villa *et al*. 2015), followed by the influx of a sedimentary fluid related to U ore deposition that produced mineralised episyenites at ~ 270 Ma. As these authors documented, the interaction of granites with hydrothermal fluids, resulted in radiogenic ^{87}Sr-loss and Rb-gain, which would be consistent with the younger than expected Rb/Sr ages and the high degree of dispersion in the data. Although causes of the wide dispersion of Rb-Sr ages of individual powder batches of Mica-Fe remain unclear, we suggest that it may result from the highly evolved and radiogenic composition of the magmas in the Saint-Sylvestre massif, the variable contents of inclusions between measured batches (~ 110 mg), especially of Sr-rich apatite and Rb-rich K-feldspar and/or ^{87}Sr-loss during the hydrothermal alteration that affected the Saint-Sylvestre granite.

The calculated two-point isochron Rb-Sr age of FK-N using the mean ^{87}Rb/^{86}Sr and ^{87}Sr/^{86}Sr ratios is 512 ± 30 Ma (Figure 8d). An estimated initial ^{87}Sr/^{86}Sr of 0.70929 was assumed, based on a whole-rock Rb-Sr isochron for pegmatite from the Kullampatti area in Tamil Nadu, southern India (Pandey *et al.* 1993). The two-point isochron ages calculated for the individual digestions of FK-N range from 503 to 528 Ma using the same assumed ^{87}Sr/^{86}Sr initial ratio. No previous age information or Rb-Sr isotope data exist for FK-N, and while this sample is known to originate in Tamil Nadu, the precise

sample location is unknown. Nevertheless, our calculated age for this RM closely matches the age of 521 ± 9 Ma of the Rb-Sr pegmatite isochron used to estimate the initial ratio (Pandey *et al*. 1993), suggesting that FK-N may also be derived from the Kullampatti area.

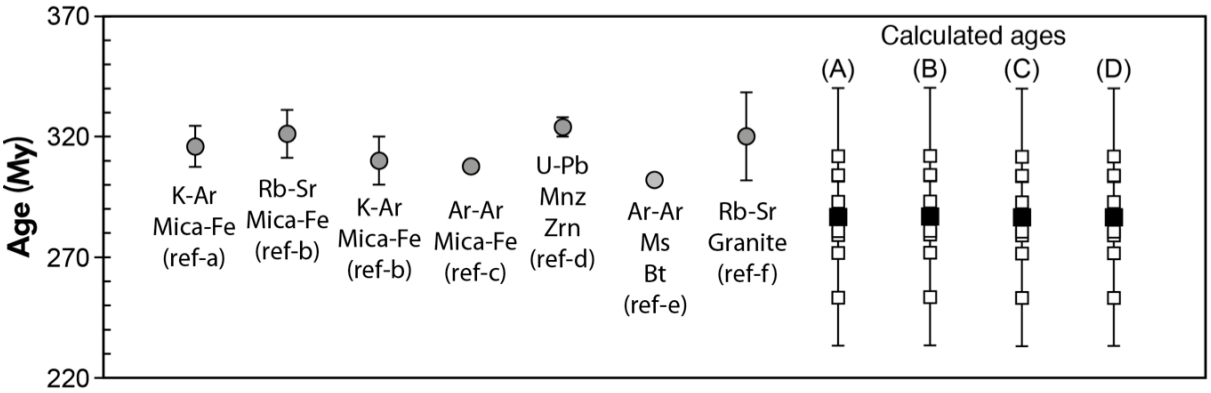

Figure 9. Two-point isochron Rb-Sr ages calculated using the measured Rb/Sr values of the mean (black square) and individual powder aliquots (white squares) for Mica-Fe compared with previously reported ages and their uncertainties as compiled in Table 1. Two assumed initial ratios of (A) 0.7074 (Duthou 1977) and (D) 0.71067 (Turpin *et al.* 1990) are used for calculated ages of Mica-Fe. Minimum and maximum initial ratios of (B) 0.7039 and (C) 0.7130 are calculated using the reported Rb-Sr isotopic data of each granite sample from Duthou (1977) and the U-Pb zircon and monazite ages of 324 ± 4 Ma (Holliger *et al.* 1986) from the Saint-Sylvestre leucogranitic complex. It is apparent that within these limits, the choice of the initial ratio has an insignificant effect on the calculated age. References presented are (a) Zimmermann *et al.* (1985), (b) Govindaraju (1979), (c) Grove and Harrison (1996), (d) Holliger *et al.* (1986), (e) Scaillet *et al.* (1996) and (f) Duthou (1977). (d) Zircon (Zrn) and monazite (Mnz), (e) muscovite (Ms) and biotite (Bt) and (f) granite are from the Saint-Sylvestre massif. The Ar-Ar plateau age from Scalillet *et al*. (1996) presented here is the mean age calculated from muscovite (302.1 ± 0.87 Ma) and biotite (302.44 ± 0.63 Ma and 301.44 ± 0.65 Ma) from the Saint-Sylvestre granite (Scaillet *et al.* 1996).

Conclusions: characterisation of the RMs for *in situ* Rb-Sr dating

This study provides working values of Rb and Sr mass fractions and Rb/Sr and Sr isotope compositions for four RMs: Mica-Mg, Mica-Fe, GL-O and FK-N. The mean $^{87}Sr/^{86}Sr$ and $^{87}Rb/^{86}Sr$ ratios are given in Table 4, along with the uncertainties that must be propagated into the total uncertainties of Rb-Sr isotopic analyses by LA-ICP-MS/MS that use these RMs for calibration. The uncertainties (2*s*) of measured Rb-Sr isotopic ratios are 4.7% for Mica-Mg, 11% for GL-O, 14% for Mica-Fe and 5.9% for FK-N, reflecting mostly the inhomogeneity of the powdered RMs. Smaller contributions to the total uncertainties come from random (in-run uncertainties, Sr blank variability, weighing errors) and systematic (spike calibration) analytical errors.

The use of appropriate matrix-matched and isotopically homogeneous RMs plays a key role in all applications of *in situ* instrumentation in geosciences. Rb-Sr dating by LA-ICP-MS/MS is one of these applications. Calibration materials of variable Rb/Sr compositions allowing matrix-matched correction for precise Rb-Sr age determination were lacking before our work. The present study provides controlled Rb and Sr mass fractions and Sr/Sr and Rb/Sr isotopic values for four natural RMs, which are chemically representative of micas and feldspars. These four RMs are available for the scientific community and can be used to calibrate LA-ICP-MS/MS data after a simple preparation stage. The availability of RMs with various chemical compositions (phlogopite, biotite, glauconite and potassium feldspar) will permit for example detailed studies of matrix effects. It will also facilitate matching pulse/analogue settings with unknown samples and calculation and propagation of analytically robust uncertainties when dating feldspars and micas by LA-ICP-MS/MS.

Among the four RMs, Mica-Fe has limitations related to its exceptionally high and heterogeneous $^{87}Rb/^{86}Sr$ and $^{87}Sr/^{86}Sr$ values, which have uncertainties (2*s*) of 14%. Mica-Fe cannot be considered as an ideal RM for calibration of biotites with less extreme Rb-Sr compositions. Development of Fe-rich mica RMs with less radiogenic values is still needed with two potential candidates: (i) biotite from the La Posta granodiorite, California (Walawender *et al.* 1990) used as a primary standard by Zack and

Hogmalm (2016) for Rb-Sr dating by LA-ICP-MS/MS and (ii) GA-1550 biotite from monazite in Mt. Dromedary (McDougall and Roksandic 1974) which was dated by several isotope systems, presenting identical ages within uncertainties (e.g., K-Ar age by Spell and McDougall 2003 and McDougall and Wellman 2011 and Rb/Sr age by Li *et al.* 2008). These two biotites were successfully tested and used in the LA-ICP-MS/MS study of Rösel and Zack (2021).

Potential Rb/Sr isotopic heterogeneity of the RMs in powder form can affect the nano-powder pellet, which is currently the best sample preparation method for Rb-Sr dating by LA-ICP-MS/MS (Hogmalm *et al.* 2017, Redaa *et al.* 2021). Sample heterogeneity of Rb/Sr ratios in the RMs is large relative to the uncertainty (2*s*) for homogenous glass standards including 0.21% for NIST SRM 610 (Wise and Watters 2012), 1.3% for NIST SRM 612 (Woodhead and Hergt 2001) and 0.23% for BCR-2G (Elburg *et al.* 2005), widely used for Rb/Sr calibration for minerals with low to medium Rb/Sr ratios. We suggest that ID-TIMS and MC-ICP-MS measurement of $^{87}Sr/^{86}Sr$ and Rb/Sr compositions should be done directly on nano-powders to define whether the procedure of producing nano-powders reduces analytical uncertainties by producing greater homogenisation of the material before isotopic analysis. Until such results become available, we recommend use of our $^{87}Sr/^{86}Sr$ and $^{87}Rb/^{86}Sr$ values and related uncertainties for the four tested RMs for *in situ* Rb-Sr dating by LA-ICP-MS/MS.

Acknowledgements

This work was supported by the French National Research Agency through the national program "Investissements d'avenir" with the reference ANR-10-LABX-21-RESSOURCES21 and the Ministry of Higher Education, Research and Innovation (MESRI) for PhD funding to Yujin Jegal. Michel Cuney is thanked for geological information concerning the massif of Saint-Sylvestre and related isotopic data. Thomas Zack is thanked for providing aliquots of NIST SRM607 K-feldspar. We thank Andreï Lecomte and Olivier Rouer (SCMEM) for their help during SEM and EPMA analyses and Aimeryc Schumacher, Christiane Parmentier, Damien Civdini (CRPG) for their assistance with MC-

ICP-MS analyses and clean lab experiments, and for fruitful discussions. We also thank Camille Kieffer, Élise Guérin and Hélène Pastel Gény (SARM-CRPG) for the ICP-MS analyses and the alkali fusion experiments. Alexandre Flammang and John Moine (Lithopreparation platforme, GeoRessources) are thanked for their help with sample preparation for SEM and EPMA analyses.

References

Armstrong R.L., Jäger E. and Eberhardt P. (1966)

A comparison of K-Ar and Rb-Sr ages on Alpine biotites. **Earth and Planetary Science Letters, 1,** 13–19.

Bolea-Fernandez E., Balcaen L., Resano M. and Vanhaecke F. (2016a)

Tandem ICP-mass spectrometry for Sr isotopic analysis without prior Rb/Sr separation. **Journal of Analytical Atomic Spectrometry, 31,** 303–310.

Bolea-Fernandez E., Van Malderen S.J., Balcaen L., Resano M. and Vanhaecke F. (2016b)

Laser ablation-tandem ICP-mass spectrometry (LA-ICP-MS/MS) for direct Sr isotopic analysis of solid samples with high Rb/Sr ratios. **Journal of Analytical Atomic Spectrometry, 31,** 464–472.

Boulesteix T., Solé J., Pi T. and Cathelineau M. (2020)

Reappraisal of the GL-O reference material for K-Ar dating: New insight from microanalysis, single-grain and milligram Ar measurements. **Geostandards and Geoanalytical Research, 44,** 287–306.

Carignan J., Hild P., Mevelle G., Morel J. and Yeghicheyan D. (2001)

Routine analyses of trace elements in geological samples using flow injection and low pressure on-line liquid chromatography coupled to ICP-MS: A study of geochemical reference materials BR, DR-

N, UB-N, AN-G and GH. **Geostandards Newsletter: The Journal of Geostandards and Geoanalysis, 25,** 187–198.

Chauvel C., Bureau S. and Poggi C. (2011)

Comprehensive chemical and isotopic analyses of basalt and sediment reference materials. **Geostandards and Geoanalytical Research, 35**, 125–143

Chen C.-H., DePaolo D.J. and Lan C.-Y. (1996)

Rb-Sr microchrons in the Manaslu granite: Implications for Himalayan thermochronology. **Earth and Planetary Science Letters, 143,** 125–135.

Cheng P., Koyanagi G.K. and Bohme D.K. (2008)

On the chemical resolution of the $^{87}Rb^{+}$ (s^{0})/$^{87}Sr^{+}$ (s^{1}) isobaric interference: A kinetic search for an optimum reagent. **Analytica Chimica Acta, 627,** 148–153.

Claverie F., Fernández B., Pécheyran C., Alexis J. and Donard O.F. (2009)

Elemental fractionation effects in high repetition rate IR femtosecond laser ablation ICP-MS analysis of glasses. **Journal of Analytical Atomic Spectrometry, 24,** 891–902.

Cuney M., Friedrich M., Blumenfeld P., Bourguignon A., Boiron M.C., Vigneresse J.L. and Poty B. (1990)

Metallogenesis in the French part of the Variscan orogen. Part I: U preconcentrations in pre-Variscan and Variscan formations – A comparison with Sn, W and Au. **Tectonophysics, 177,** 39–57.

Duthou J.L. (1977)

Chronologie Rb-Sr et geochimie des granitoides d'un segment de la chaine varisque, relations avec le metamorphisme: le Nord limousin, Massif central francais. **Universite de Clermont, Unite d'enseignement et de recherche de sciences**

Eberlei T., Habler G., Wegner W., Schuster R., Körner W., Thöni M. and Abart R. (2015)

Rb/Sr isotopic and compositional retentivity of muscovite during deformation. **Lithos, 227,** 161–178.

Elburg M., Vroon P., van der Wagt B. and Tchalikian A. (2005)

Sr and Pb isotopic composition of five USGS glasses (BHVO-2G, BIR-1G, BCR-2G, TB-1G, NKT-1G). **Chemical Geology, 223,** 196–207.

Farina F., Dini A., Rocchi S. and Stevens G. (2014)

Extreme mineral-scale Sr isotope heterogeneity in granites by disequilibrium melting of the crust. **Earth and Planetary Science Letters, 399,** 103–115.

Fletcher I., McNaughton N., Pidgeon R. and Rosman K. (1997)

Sequential closure of K–Ca and Rb–Sr isotopic systems in Archaean micas. **Chemical Geology, 138,** 289–301.

Freeman S., Inger S., Butler R. and Cliff R. (1997)

Dating deformation using Rb-Sr in white mica: Greenschist facies deformation ages from the Entrelor shear zone, Italian Alps. **Tectonics, 16,** 57–76.

Friedrich M. (1983)

Le complexe granitique hyperalumineux de Saint Sylvestre, nord-ouest du Massif central français: évolution de la cristallochimie des phases minérales et de la géochimie des éléments en trace et

majeurs; caractérisation du polygénisme dans les granites hyperalumineux; implications sur la métallogénie de l'uranium. Thèse de doctorat de troisième cycle. **Université de Nancy I**.

Friedrich M., Cuney M. and Poty B. (1987)

Uranium geochemistry in peraluminous leucogranites. **Uranium, 3,** 353–385.

Glodny J., Bingen B., Austrheim H., Molina J.F. and Rusin A. (2002)

Precise eclogitization ages deduced from Rb/Sr mineral systematics: The Maksyutov complex, Southern Urals, Russia. **Geochimica et Cosmochimica Acta, 66,** 1221–1235.

Glodny J., Kühn A. and Austrheim H. (2008)

Diffusion versus recrystallization processes in Rb–Sr geochronology: Isotopic relics in eclogite facies rocks, Western Gneiss Region, Norway. **Geochimica et Cosmochimica Acta, 72,** 506–525.

Gorojovsky L. and Alard O. (2020)

Optimisation of laser and mass spectrometer parameters for the *in situ* analysis of Rb/Sr ratios by LA-ICP-MS/MS. **Journal of Analytical Atomic Spectrometry, 35,** 2322–2336.

Govindaraju K. (1979)

Report (1968–1978) on two mica reference samples: Biotite Mica-Fe and Phlogopite Mica-Mg. **Geostandards Newsletter, 3,** 3–24.

Govindaraju K. (1984)

Report (1973–1984) on two ANRT geochemical reference samples: Granite GS-N and Potash Feldspar FK-N. **Geostandards Newsletter, 8,** 173–206.

Govindaraju K. (1995)

1995 Working values with confidence limits for twenty-six CRPG, ANRT AND IWG-GIT gesotandards. **Geostandards Newsletter, 19 (Special Issue),** 32pp.

Grove M. and Harrison T. (1996)

Diffusion in ^{40*}Ar Fe-rich phlogopite. **American Mineralalogist, 81,** 940–951.

Hogmalm K.J., Zack T., Karlsson A.K.-O., Sjöqvist A.S. and Garbe-Schönberg D. (2017)

In situ Rb–Sr and K–Ca dating by LA-ICP-MS/MS: an evaluation of N_2O and SF_6 as reaction gasses. **Journal of Analytical Atomic Spectrometry, 32,** 305–313.

Holliger P., Cuney M., Friedrich M. and Turpin L. (1986)

U-Pb carboniferous age on zircons and monazites from the Brame unit of the Saint-Sylvestre peraluminous granitic complex (NW Massif Central, France). **Comptes Rendus des Seances de l'Academie des Sciences. Serie 2, 303,** 1309–1314.

Jackson S.E. and Günther D. (2003)

The nature and sources of laser induced isotopic fractionation in laser ablation-multicollector-inductively coupled plasma-mass spectrometry. **Journal of Analytical Atomic Spectrometry, 18,** 205–212.

Jackson S.E. and Sylvester P. (2008)

Calibration strategies for elemental analysis by LA-ICP-MS. **Signal, 10,** 100.

Kröner A., Braun I. and Jaeckel P. (1996)

Zircon geochronology of anatectic melts and residues from a highgrade pelitic assemblage at Ihosy, southern Madagascar: Evidence for Pan-African granulite metamorphism. **Geological Magazine, 133,** 311–323.

Laureijs C.T., Coogan L.A. and Spence J. (2021)

A high throughput Rb-Sr dating method using solution tandem ICP-MS/MS ($^{87}Sr/^{86}Sr$) and standard addition calibration ICP-MS (Rb/Sr). **MethodsX, 8,** 101309.

Li Q.-L., Chen F., Li X.-H., Wang F. and He H.-Y. (2008)

Single grain Rb-Sr isotopic analysis of GA-1550 biotite, LP-6 biotite and Bern-4M muscovite ^{40}Ar-^{39}Ar dating standards. **Geochemical Journal, 42,** 263–271.

Li Q., Chen F., Wang X., Li X. and Li C. (2005)

Ultra-low procedural blank and the single-grain mica Rb-Sr isochron dating. **Chinese Science Bulletin, 50,** 2861–2865.

Li S.-S., Santosh M., Farkaš J., Redaa A., Ganguly S., Kim S.W., Zhang C., Gilbert S. and Zack T. (2020)

Coupled U-Pb and Rb-Sr laser ablation geochronology trace Archean to Proterozoic crustal evolution in the Dharwar Craton, India. **Precambrian Research, 343,** 105709.

Liu X., Dong S., Yue Y., Guan Q., Sun Y., Chen S., Zhang J. and Yang Y. (2020)

$^{87}Sr/^{86}Sr$ isotope ratios in rocks determined using inductively coupled plasma tandem mass spectrometry in O_2 mode without prior Sr purification. **Rapid Communications in Mass Spectrometry, 34,** e8690.

Liu Y., Hu Z., Li M. and Gao S. (2013)

Applications of LA-ICP-MS in the elemental analyses of geological samples. **Chinese Science Bulletin, 58,** 3863–3878.

Martin R.F., Randrianandraisana A. and Boulvais P. (2014)

Ampandrandava and similar phlogopite deposits in southern Madagascar: Derivation from a silicocarbonatitic melt of crustal origin. **Journal of African Earth Sciences, 94,** 111–118.

McDougall I. and Roksandic Z. (1974)

Total fusion $^{40}Ar/^{39}Ar$ ages using HIFAR reactor. **Journal of the Geological Society of Australia, 21,** 81-89.

McDougall I. and Wellman P. (2011)

Calibration of GA1550 biotite standard for K/Ar and $^{40}Ar/^{39}Ar$ dating. **Chemical Geology, 280,** 19–25.

Moens L., Vanhaecke F., Bandura D., Baranov V. and Tanner S. (2001)

Elimination of isobaric interferences in ICP-MS, using ion–molecule reaction chemistry: Rb/Sr age determination of magmatic rocks, a case study. **Journal of Analytical Atomic Spectrometry, 16,** 991–994.

Morteani G., Kostitsyn Y., Gilg H., Preinfalk C. and Razakamanana T. (2013)

Geochemistry of phlogopite, diopside, calcite, anhydrite and apatite pegmatites and syenites of southern Madagascar: evidence for crustal silicocarbonatitic (CSC) melt formation in a Panafrican collisional tectonic setting. **International Journal of Earth Sciences, 102,** 627–645.

Nebel O. (2014)

Rb–Sr Dating. **In: Rink W.J. and Thompson J. (eds), Encyclopedia of Scientific Dating Methods. Springer Netherlands (Dordrecht),** 1–19.

Nebel O. and Mezger K. (2006)

Reassessment of the NBS SRM-607 K-feldspar as a high precision Rb/Sr and Sr isotope reference. **Chemical Geology, 233,** 337–345.

Nebel O., Mezger K., Scherer E. and Münker C. (2005)

High precision determinations of $^{87}Rb/^{85}Rb$ in geologic materials by MC-ICP-MS. **International Journal of Mass Spectrometry, 246,** 10–18.

Odin G.S. A.C.J., Armstrong R.L., Bagdasaryan G.P., Baksi A.K., Balogh K., Barnes N.A., Boelrijk I.M., Bonadonna F.P., Bonhomme M.G., Cassignol C., Chanin L., Gillot P.Y., Gledhill A., Govindaraju K., Harakal R., Harre W., Hebeda E.H., Hunziker J.C., Ingamells C.O., Kawashita K., Kiss E., Kreuzer H., Long L.E., McDougall I., McDowell F., Mehnert H., Montigny R., Pasteels P., Radicati F., Rex D.C., Rundle C.C., Savelli C., Sonet J., Welin E. and Zimmermann J.L. (1982)

Intel-laboratory standards for dating purposes. **In: Odin G.S. (ed.), Numerical dating in stratigraphy,** 123–149.

Olierook H.K., Rankenburg K., Ulrich S., Kirkland C.L., Evans N.J., Brown S., McInnes B.I., Prent A., Gillespie J. and McDonald B. (2020)

Resolving multiple geological events using *in situ* Rb–Sr geochronology: Implications for metallogenesis at Tropicana, Western Australia. **Geochronology, 2,** 283–303.

Pandey B., Krishna V., Sastry D., Chabria T., Mary K. and Dhanaraju R. (1993)

Pan-African wholerock Rb–Sr isochron ages for the granites and pegmatites of Kullampatti–Suriyamalai area, Salem District, Tamil Nadu, India. **Mass Spectrometry'IIP, Dehra Dun,** 480–482.

Redaa A., Farkaš J., Gilbert S., Collins A.S., Wade B., Löhr S., Zack T. and Garbe-Schönberg D. (2021)

Assessment of elemental fractionation and matrix effects during *in situ* Rb–Sr dating of phlogopite by LA-ICP-MS/MS: Implications for the accuracy and precision of mineral ages. **Journal of Analytical Atomic Spectrometry, 36,** 322–344.

Rodushkin I., Axelsson M.D., Malinovsky D. and Baxter D.C. (2002)

Analyte- and matrix-dependent elemental response variations in laser ablation inductively coupled plasma-mass spectrometry. **Journal of Analytical Atomic Spectrometry, 17,** 1223–1230.

Rösel D. and Zack T. (2021)

LA-ICP-MS/MS single spot Rb-Sr dating. **Geostandards and Geoanalytical Research, 46**, 143–168.

Roy M. and Raju R.D. (1999)

Petrogenetic model of A-type granitoids of the Kullampatti area, Salem district, Tamil Nadu, India. **Gondwana Research, 2,** 127–135.

Scaillet S., Cheilletz A., Cuney M., Farrar E. and Archibald D. (1996)

Cooling pattern and mineralization history of the Saint Sylvestre and western Marche leucogranite pluton, French Massif Central: I. $^{40}Ar/^{39}Ar$ isotopic constraints. **Geochimica et Cosmochimica Acta, 60,** 4653–4671.

Şengün F., Bertrandsson Erlandsson V., Hogmalm J. and Zack T. (2019)

In situ Rb-Sr dating of K-bearing minerals from the orogenic Akçaabat gold deposit in the Menderes Massif, western Anatolia, Turkey **Journal of Asian Earth Sciences, 185,** 104048.

Smith P.E., Evensen N.M., York D. and Odin G.S. (1998)

Single-Grain ^{40}Ar- ^{39}Ar ages of glauconies: Implications for the geologic time scale and global sea level variations. **Science, 279,** 1517–1519.

Spell T.L. and McDougall I. (2003)

Characterization and calibration of $^{40}Ar/^{39}Ar$ dating standards. **Chemical Geology, 198,** 189–211.

Tillberg M., Drake H., Zack T., Hogmalm J. and Åström M. (2017)

In situ Rb-Sr dating of fine-grained vein mineralizations using LA-ICP-MS **Procedia Earth and Planetary Science, 17,** 464–467.

Tillberg M., Drake H., Zack T., Kooijman E., Whitehouse M.J. and Åström M.E. (2020)

In situ Rb-Sr dating of slickenfibres in deep crystalline basement faults. **Scientific reports, 10,** 1–13.

Turpin L., Leroy J.L. and Sheppard S.M. (1990)

Isotopic systematics (O, H, C, Sr, Nd) of superimposed barren and U-bearing hydrothermal systems in a Hercynian granite, Massif Central, France. **Chemical Geology, 88,** 85–98.

Uhlig D., Amelung W. and Von Blanckenburg F. (2020)

Mineral nutrients sourced in deep regolith sustain long-term nutrition of mountainous temperate forest ecosystems. **Global Biogeochemical Cycles, 34**, e2019GB006513.

Vanhaecke F., De Wannemacker G., Moens L. and Hertogen J. (1999)

The determination of strontium isotope ratios by means of quadrupole-based ICP-mass spectrometry: a geochronological case study. **Journal of Analytical Atomic Spectrometry, 14,** 1691–1696.

Vermeesch P. (2018)

IsoplotR: A free and open toolbox for geochronology. **Geoscience Frontiers, 9,** 1479–1493.

Villa I.M., De Bièvre P., Holden N.E. and Renne P.R. (2015)

IUPAC-IUGS recommendation on the half life of ^{87}Rb. **Geochimica et Cosmochimica Acta, 164,** 382–385.

Villaros A. and Pichavant M. (2019)

Mica-liquid trace elements partitioning and the granite-pegmatite connection: The St-Sylvestre complex (western French Massif Central). **Chemical Geology, 528,** 119265.

Waight T., Baker J. and Willigers B. (2002)

Rb isotope dilution analyses by MC-ICPMS using Zr to correct for mass fractionation: towards improved Rb–Sr geochronology? **Chemical Geology, 186,** 99–116.

Walawender M., Gastil R., Clinkenbeard J., McCormick W., Eastman B., Wemicke R., Wardlaw M., Gunn S. and Smith B. (1990)

Origin and evolution of the zoned La Posta-type plutons, eastern Peninsular. **The nature and origin of Cordilleran Magmatism, 174,** 1.

Willigers B., Mezger K. and Baker J. (2004)

Development of high precision Rb–Sr phlogopite and biotite geochronology: An alternative to ^{40}Ar/^{39}Ar tri-octahedral mica dating. **Chemical Geology, 213,** 339–358.

Wise S.A. and Watters R.L. (2012)

Certificate of analysis: Standard Reference Material 610. **National Institute of Standards and Technology (Gaithersburg, USA).**

Woodhead J.D. and Hergt J.M. (2001)

Strontium, neodymium and lead isotope analyses of NIST glass certified reference materials: SRM 610, 612, 614. **Geostandards Newsletter: The Journal of Geostandards and Geoanalysis, 25,** 261–266.

Zack T. and Hogmalm K.J. (2016)

Laser ablation Rb/Sr dating by online chemical separation of Rb and Sr in an oxygen-filled reaction cell. **Chemical Geology, 437,** 120–133.

Zhang S., He M., Yin Z., Zhu E., Hang W. and Huang B. (2016)

Elemental fractionation and matrix effects in laser sampling based spectrometry. **Journal of Analytical Atomic Spectrometry, 31,** 358–382.

Zimmermann J., Vernet M., Guyetand G. and Dautel D. (1985)

Données sur potassium et argon (de 1976 à 1984) dans quelques échantillons géochimiques de référence. **Geostandards Newsletter, 9,** 205–208.

Supporting information

The following supporting information may be found in the online version of this article:

Figure S1. $^{87}Sr/^{86}Sr$ compositions of Sr blanks.

Figure S2a-h. BSE images and SEM-EDS (Figs. S2b, e, g), and EPMA (Figs. S2a, c, d, f) elemental maps for Mica-Mg phlogopite grains (grain# a, b, c, e, g, h, i, h).

Figure S3. BSE images of GL-O glauconite grains. Yellow squares represent locations of 10 x 10µm defocused analyses by EPMA (**Table S6**).

Figure S4a-e. BSE image and SEM-EDS (Figs. S4c, d, e), and EPMA (Figs. S4a, b) elemental maps for Mica-Fe biotite grains (grain# a, b, c, d, g).

Figure S5a-e. BSE image and SEM-EDS (Figs. S5a, b, c, d, e) elemental maps for FK-N potassium feldspar grains (grain# a, b, d, e, f).

Figure S6. $^{87}Rb/^{86}Sr$ and $^{87}Sr/^{86}Sr$ isotope compositions of Mica-Fe in this study and the Rb-Sr isotopic data of biotites (sample B1355 and B1354) from Duthou (1977). The two-point isochron Rb-Sr ages for sample B1355 and B1354 are calculated using the assumed initial ratio of 0.7074 from Duthou (1977).

Table S1. Powdered and solid reference materials used in this study

Table S2. Rb-Sr mass fractions and $^{87}Sr/^{86}Sr$ ratios for the secondary standards compared with literature values

Table S3. Absolute quantities (ng) of Rb and Sr in the samples analysed by ID-TIMS and MC-ICP-MS (this study) in **Table 3**.

Table S4. Mean Sr, Rb/Sr, $^{87}Rb/^{86}Sr$, and $^{87}Sr/^{86}Sr$ values and corresponding ages for each RM calculated using different assumptions for the Sr blank contribution.

Table S5. EPMA compositions of Mica-Mg grains

Table S6. EPMA compositions of GL-O grains

Table S7. EPMA compositions of Mica-Fe flakes

Table S8. EPMA compositions of FK-N grains

Table S9. Rb and Sr mass fractions of the RMs determined by alkali fusion followed by ICP-MS analysis

Table captions

Table 1. Previously reported ages for the samples and for their host rocks or associated deposits with Rb-Sr model ages of the samples in this study.

Table 2. ^{85}Rb and ^{84}Sr (M/g) of the ^{85}Rb and ^{84}Sr spikes, respectively, and uncertainties (2*s*%). The uncertainties of the Rb spikes are total values that include both the variation of replicate spike calibration measurements and uncertainties on the concentrations of the solutions used for calibration. The ^{85}Rb and ^{84}Sr spikes were added separately in differing amounts depending on the sample composition.

Table 3. Rb-Sr mass fractions and $^{87}Sr/^{86}Sr$ ratios of (a) Mica-Mg, (b) GL-O and FK-N and (c) Mica-Fe for repeat analyses of the studied RMs compared with literature values.

Table 4. Working values and uncertainties for the RMs in this study.